© 2023. Published by The Company of Biologists Ltd | Biology Open (2023) 12, bio060113. doi:10.1242/bio.060113

RESEARCH ARTICLE

Deficiency of the Heterogeneous Nuclear Ribonucleoprotein U locus leads to delayed hindbrain neurogenesis

Francesca Mastropasqua[1,2,*], Marika Oksanen[1,2,*], Cristina Soldini[1,2], Shemim Alatar[1,2], Abishek Arora[1,2], Roberto Ballarino[3,4,5], Maya Molinari[6], Federico Agostini[4,5], Axel Poulet[7], Michelle Watts[1,2], Ielyzaveta Rabkina[1,2], Martin Becker[1,2], Danyang Li[1,2], Britt-Marie Anderlid[8,9], Johan Isaksson[1,10], Karl Lundin Remnelius[1], Mohsen Moslem[6], Yannick Jacob[7], Anna Falk[6,11], Nicola Crosetto[3,4,12], Magda Bienko[3,4,12], Emanuela Santini[6], Anders Borgkvist[6], Sven Bölte[1,2,13,14] and Kristiina Tammimies[1,2,‡]

ABSTRACT

Genetic variants affecting *Heterogeneous Nuclear Ribonucleoprotein U* (*HNRNPU*) have been identified in several neurodevelopmental disorders (NDDs). HNRNPU is widely expressed in the human brain and shows the highest postnatal expression in the cerebellum. Recent studies have investigated the role of *HNRNPU* in cerebral cortical development, but the effects of *HNRNPU* deficiency on cerebellar development remain unknown. Here, we describe the molecular and cellular outcomes of *HNRNPU* locus deficiency during *in vitro* neural differentiation of patient-derived and isogenic neuroepithelial stem cells with a hindbrain profile. We demonstrate that *HNRNPU* deficiency leads to chromatin remodeling of A/B compartments, and transcriptional rewiring, partly by impacting exon inclusion during mRNA processing. Genomic regions affected by the chromatin restructuring and host genes of exon usage differences show a strong enrichment for genes implicated in epilepsies, intellectual disability, and autism. Lastly, we show that at the cellular level HNRNPU downregulation leads to an increased fraction of neural progenitors in the maturing neuronal population. We conclude that the *HNRNPU* locus is involved in delayed commitment of neural progenitors to differentiate in cell types with hindbrain profile.

KEY WORDS: HNRNPU, Neurodevelopmental disorders, Neurogenesis, Hindbrain, HiC-sequencing, RNA-sequencing

INTRODUCTION

Enormous progress in genomic technologies has led to the discovery of hundreds of genes associated with various neurodevelopmental disorders (NDDs). These include several genes belonging to the heterogeneous nuclear ribonucleoprotein (hnRNP) family (Gillentine et al., 2021). One of the genes within this family, *HNRNPU*, which encodes for Heterogeneous Nuclear Ribonucleoprotein U [also known as Scaffold Attachment Factor A (SAF-A)] (Kiledjian and Dreyfuss, 1992), has emerged as a frequently affected gene leading to NDDs such as intellectual disability (ID), autism spectrum disorder (ASD) as well as neurological conditions such as epilepsies (Depienne et al., 2017; Satterstrom et al., 2020; Taylor et al., 2022). The gene was first indicated in NDDs as part of the 1q44 microdeletion syndrome characterized by a severe global developmental delay, ID, seizures, muscular hypotonia, hearth, and congenital malformations such as agenesis of the corpus callosum, heart and skeletal anomalies (Depienne et al., 2017). Later, several smaller deletions and point mutations affecting the *HNRNPU* locus pinpointed it as the causal gene within the locus for the majority of the brain-related phenotypes (Bramswig et al., 2017; Leduc et al., 2017; Shimojima et al., 2012; Tung et al., 2021; Yates et al., 2017). In addition to the *HNRNPU* gene, a long non-coding RNA *HNRNPU-AS1* maps to the locus. The function of *HNRNPU-AS1* is not known, although some reports have indicated its role in different molecular pathways, such as cell proliferation and apoptosis in cancer cells (Niu et al., 2021; Zhang et al., 2022). To date, several reports exist about the pathogenic genetic variants affecting the *HNRNPU* gene in individuals with *HNRNPU*-related disorder, and are mostly *de novo* loss-of-function variants at sequence or copy number level (Brunet et al., 2021; Durkin et al., 2020; Gillentine et al., 2021; Wang et al., 2020). All the reported cases are heterozygous variants, suggesting that homozygous gene-disrupting variants affecting *HNRNPU* are embryonic lethal in humans, similar to what has been demonstrated in mice (Dugger et al., 2020; Roshon and Ruley, 2005; Ye et al., 2015).

HNRNPU has a key role in three-dimensional (3D) genome organization and regulating RNA processing (Fan et al., 2018; Marenda et al., 2022; Nozawa et al., 2017; Xiong et al., 2020;

[1]Center of Neurodevelopmental Disorders (KIND), Centre for Psychiatry Research, Department of Women's and Children's Health, Karolinska Institute, Region Stockholm, 17164 Stockholm, Sweden. [2]Astrid Lindgren Children's Hospital, Karolinska University Hospital, Region Stockholm, 17164 Stockholm, Sweden. [3]Department of Microbiology, Tumor and Cell Biology, Karolinska Institutet, 17164 Stockholm, Sweden. [4]Science for Life Laboratory, Tomtebodavägen 23A, 17165 Solna, Sweden. [5]Department of Medical Biochemistry and Biophysics, Karolinska Institutet, 17165 Stockholm, Sweden. [6]Department of Neuroscience, Karolinska Institutet, 17176 Solna, Sweden. [7]Department of Molecular, Cellular and Developmental Biology, Yale University, New Haven, CT 06511, USA. [8]Department of Molecular Medicine and Surgery, Karolinska Institutet, 17177 Stockholm, Sweden. [9]Department of Clinical Genetics, Karolinska University Hospital, 17164 Stockholm, Sweden. [10]Department of Medical Sciences, Child and Adolescent Psychiatry Unit, Uppsala University, 75309 Uppsala, Sweden. [11]Lund Stem Cell Center, Lund University, 22100 Lund, Sweden. [12]Human Technopole, Viale Rita Levi-Montalcini 1, 20157 Milan, Italy. [13]Curtin Autism Research Group, Curtin School of Allied Health, Curtin University, 6845 Perth, Western Australia. [14]Child and Adolescent Psychiatry, Stockholm Health Care Services, Region Stockholm, 10431 Stockholm, Sweden.
*These authors contributed equally to this work

‡Author for correspondence (kristiina.tammimies@ki.se)

F.M., 0000-0003-4237-2446; M.O., 0000-0003-4140-4282; S.A., 0009-0009-0738-2340; A.A., 0000-0002-6149-4417; R.B., 0000-0001-7812-0940; F.A., 0000-0002-5453-2737; A.P., 0000-0002-3415-8960; M.W., 0000-0002-3178-3429; I.R., 0000-0001-5890-4115; M.B., 0000-0001-8442-4246; D.L., 0000-0001-7470-6645; B.-M.A., 0000-0002-2488-6024; J.I., 0000-0003-1033-2618; Y.J., 0000-0003-4741-0755; A.F., 0000-0003-1634-8610; N.C., 0000-0002-3019-6978; M.B., 0000-0002-6499-9082; E.S., 0000-0002-8948-9652; A.B., 0000-0003-1698-0288; S.B., 0000-0002-4579-4970; K.T., 0000-0002-8324-4697

Received 25 August 2023; Accepted 4 September 2023

Biology Open (2023) 12, bio060113. doi:10.1242/bio.060113

Ye et al., 2015). For instance, HNRNPU modulates chromatin compaction by promoting chromatin accessibility in a dynamic yet structured fashion, dependent on its oligomerization status (Nozawa et al., 2017). Recent studies have also shown the involvement of HNRNPU in mitosis and cell division by changing its interactions with condensed chromatin and influencing DNA replication and sister chromatid separation (Connolly et al., 2022; Ma et al., 2011; Sharp et al., 2020). Several studies have reported a role for HNRNPU in splicing, promoting both exon inclusion and exclusion (Huelga et al., 2012; Jones et al., 2022; Ye et al., 2015). Mechanistically, it has been shown that HNRNPU can stabilize the pre-mRNA structure, thus inhibiting the splicing of certain exons (Jones et al., 2022). A critical role for Hnrnpu-mediated splicing has also been demonstrated during pre- and postnatal heart development in mice, showing that loss of *Hnrnpu* leads to increased intron retention events, causing abnormality in heart development and function (Ye et al., 2015).

Recently, few studies shed light on the effects of *HNRNPU* mutations in cortical development. A mouse model of *Hnrnpu* haploinsufficiency presented abnormal brain organization and showed at postnatal day 0 altered transcriptome with downregulation of pathways related to neuronal projection and migration and upregulation of genes relevant to cell growth and protein localization in hippocampal and neocortical cells (Dugger et al., 2020). In contrast, a study performed on embryonic mice upon complete conditional *Hnrnpu* knockout in the cerebral cortex showed upregulation of genes involved in synaptic activity and downregulation of DNA-related ontologies together with changes in alternative splicing regulation (Sapir et al., 2022). Similarly, an isogenic human cortex organoid model with two clonal cell lines carrying different heterozygous mutations in *HNRNPU* partially resembled what was observed in the embryonic mice but not the postnatal model (Ressler et al., 2023). Therefore, the overall outcome of *HNRNPU* genetic variants might depend on the stage of development, brain region studied, genetic background, and gene dosage.

So far, the studies have mainly focused on cortex development and forebrain structures. *HNRNPU* is expressed in different tissues, and postnatally it is highest in cerebellum (Thierry et al., 2012). Accordingly, atrophy of the cerebellum was highlighted in a cohort of patients affected by *HNRNPU*-related disorder (Durkin et al., 2020). The cerebellum is one of the most studied hindbrain structures, and has emerged as important for typical and atypical development, and abnormalities in cerebellar development have been associated with ASD and ID (Burstein and Geva, 2021; Frosch et al., 2022; Spahiu et al., 2022). Recent observations have highlighted the influence of hindbrain development on the brain cortex and its pivotal role for cognitive functions (Joseph, 2000; Kohlmeier and Polli, 2020) and suggested that analysis of midbrain and hindbrain are needed to expand the knowledge about NDDs (London et al., 2022).

Here, we focused on delineating the molecular and cellular consequences of the *HNRNPU* locus deficiency in a model of human early hindbrain development using induced pluripotent stem cells (iPSCs) from an individual with *HNRNPU*-related disorder and a knockdown isogenic cell approach for comparative analyses, and providing evidence of a broad spectrum of affected pathways.

RESULTS

Generation and characterization of *HNRNPU* locus knockdown in iPS and neuroepithelial stem cells

To assess the molecular effects of *HNRNPU* locus (including *HNRNPU* and *HNRNPU-AS1*) haploinsufficiency during human hindbrain differentiation, we generated two different *HNRNPU* locus deficient cellular models derived from human iPSCs. The iPSCs were induced into neuroepithelial stem (NES) cells with hindbrain profile and further differentiated for 5 (D5) and 28 (D28) days using an undirected protocol as previously described (Becker et al., 2020; Falk et al., 2012) (Fig. 1A-B). This approach generates a cell culture consisting of a mixed population of cells expressing excitatory, inhibitory, and progenitor neural cell markers representing a physiological neuronal environment (Falk et al., 2012).

We first generated an *HNRNPU*-related disorder patient cell model, hereafter called HNRNPU$_{del/+}$. Through genetic screening of a twin cohort focusing on NDDs, we identified a male twin pair carrying a 44 kilobase (kb) heterozygous deletion spanning from *COX20* to *HNRNPU* genes (Stamouli et al., 2018). The twins were diagnosed with ASD, ID, and fever-induced seizures. A detailed phenotypic description of the twin pair is presented in Table S1. As *COX20* deficiency is an autosomal recessive disorder, we estimated that the effect of heterozygous deletion of *COX20* would not have a major role in the cellular phenotype (Ban et al., 2022). We obtained fibroblasts from skin biopsies of the twins and while the reprogramming of the fibroblasts from twin-1 was not effective, we successfully reprogrammed twin-2 fibroblasts into iPSCs. The iPSCs had a normal karyotype, pluripotent marker expression and showed significant reduction of *HNRNPU* and *HNRNPU-AS1* compared with control iPSCs (Fig. 1C; Fig. S1A, S1B). In addition, we used dual-SMAD inhibition to derive NES cells from the iPSCs as previously described (Falk et al., 2012), followed by staining for neural stem cell markers Nestin and SRY (sex determining region Y)-box 2 (SOX2) to verify their identity (Fig. S1C). To confirm the downregulation of *HNRNPU*-related RNA and protein product, we measured *HNRNPU-AS1* RNA, and *HNRNPU* RNA and protein in HNRNPU$_{del/+}$ cells using cells obtained from a neurotypical male control (CTRL) (Uhlin et al., 2017a) as a reference. HNRNPU$_{del/+}$ showed significantly lower RNA expression for both *HNRNPU-AS1* and *HNRNPU* ($P<1.0\times10^{-5}$, ANOVA and post hoc Tukey test) and an average lower expression of HNRNPU protein spanning from ∼20% to ∼60% downregulation (Fig. 1D-F).

As a complementary approach, we generated an isogenic cell model, hereafter called siHNRNPU, in which we reduced *HNRNPU-AS1* RNA, and *HNRNPU* RNA and protein expression using a pool of small interfering RNA (siRNA) oligos in CTRL cells in parallel with non-target oligo pool (siNTC), similar to approaches successfully used in previous studies of HNRNPU in other cell types (Ma et al., 2011; Nozawa et al., 2017; Zietzer et al., 2020). To achieve consistent knockdown of *HNRNPU* throughout differentiation, we performed repetitive siRNA treatments every 6 days. Significant downregulation of *HNRNPU-AS1* and *HNRNPU* RNA and a 32% reduction of HNRNPU protein expression were observed at NES stage. Both transcripts were similarly significantly downregulated at D5, but no significant difference was observed in *HNRNPU* RNA expression after 28 days in differentiation either by RNA sequencing (RNA-seq) or real-time PCR (Fig. S1D). Nonetheless, HNRNPU protein expression was reduced to 29% at D28 compared with siNTC samples (Fig. S1G), therefore, we considered the silencing successful and proceeded with further analyses. The *HNRNPU-AS1* was consistently downregulated after differentiation (Fig. S1D).

Our results of the variable RNA and protein expressions after downregulation of *HNRNPU* by siRNA treatment or mutation are consistent with all the previous studies about *HNRNPU* mutations in brain tissues and differentiated neuronal populations (Dugger et al.,

Biology Open (2023) 12, bio060113. doi:10.1242/bio.060113

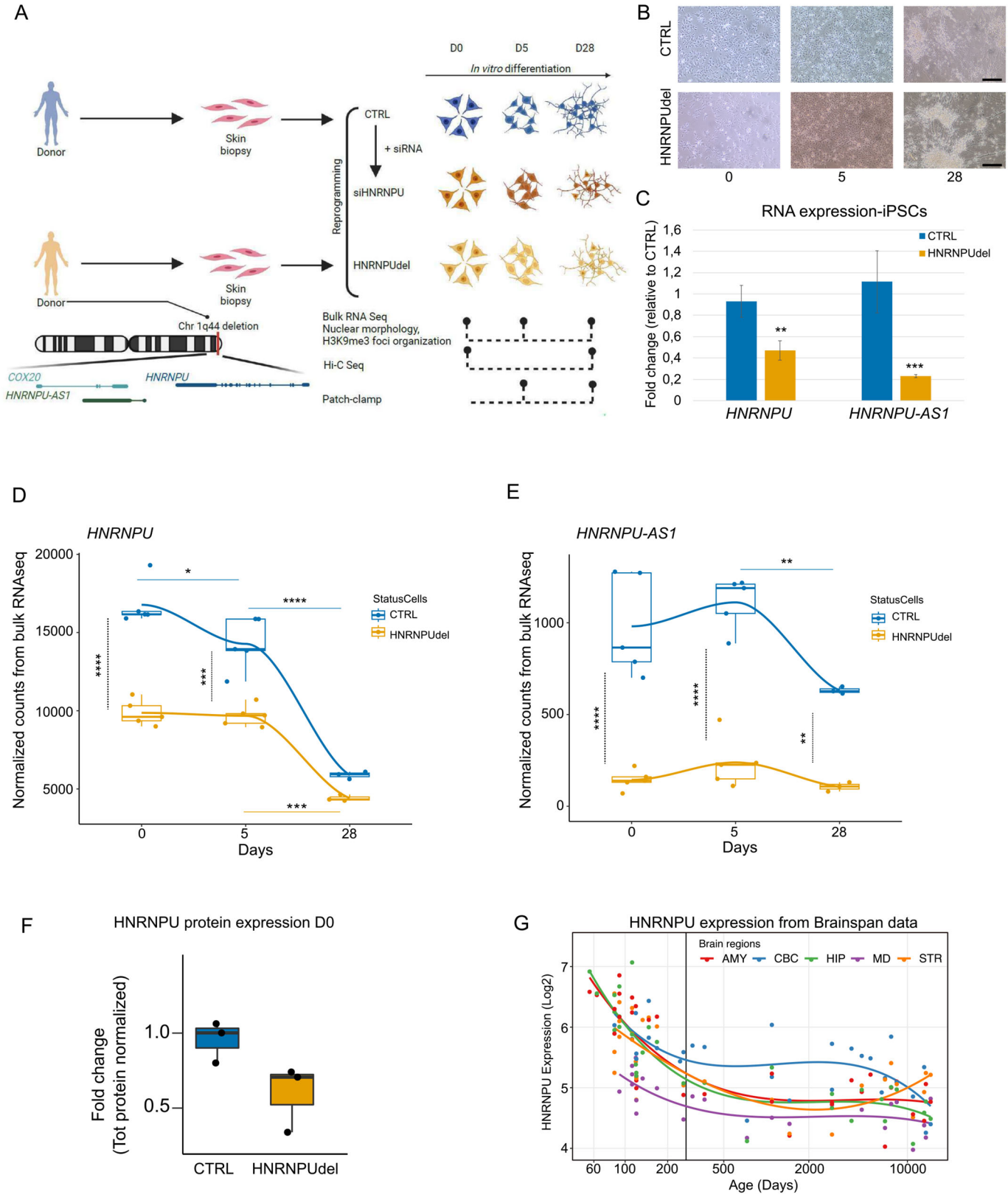

Fig. 1. *HNRNPU* expression changes during neural differentiation and brain development. (A) Schematic summary of the samples and methods used in the study (created with BioRender.com). (B) Brightfield microscopy of CTRL and HNRNPU$_{del/+}$ cells at D0, D5, D28. Scale bar: 50 µm. (C) *HNRNPU* and *HNRNPU-AS1* RNA expression in CTRL and HNRNPU$_{del/+}$ iPSC cells. (D-E) *HNRNPU* (D) and *HNRNPU-AS1* (E) RNA expression in CTRL and HNRNPU$_{del/+}$ at D0, D5, D28. The full lines indicate the comparisons between the time points for each cell line; the black dotted line indicates the comparison between the two cell lines at each time point. (F) HNRNPU protein expression in CTRL and HNRNPU$_{del/+}$ at D0. (G) *HNRNPU* RNA expression in all the brain regions during development from Human Brain Transcriptome dataset. The vertical line indicates the time of birth. AMY, amygdala; CBC, cerebellar cortex; HIP, hippocampus; MD, mediodorsal nucleus thalamus; STR, striatum; *P<0.05; **P<1×10^{-3}; ***P<1×10^{-4}; ****P<1×10^{-5}. HNRNPU$_{del/+}$ samples are indicated as 'HNRNPUdel'.

Biology Open (2023) 12, bio060113. doi:10.1242/bio.060113

2020; Ressler et al., 2023; Sapir et al., 2022). Even after knockdown or knockout at gene level, these studies showed that *HNRNPU* expression levels are similar to the wild-type controls suggesting possible compensatory mechanisms. A possible mechanism might reside in the capacity of proteins belonging to the HNRNP family to directly associate with their own transcripts, thus stabilizing them (Huelga et al., 2012). For instance, single-cell RNA transcriptome comparison of human cortical organoids carrying two different frameshift mutations in *HNRNPU* revealed no difference in HNRNPU expression between the HNRNPU-mutant and relative control, in any of the identified cell types. At the same time, the downregulation of *HNRNPU* at the RNA level does not always translate into a similar reduction at the protein level (Dugger et al., 2020; Ressler et al., 2023; Sapir et al., 2022).

HNRNPU expression changes during hindbrain neural differentiation and brain development

Next, we sought to analyze the molecular consequences of *HNRNPU* haploinsufficiency during human hindbrain development. We extracted total RNA for transcriptomic analyses from NES cells collected at three different time points of differentiation (D0, D5, and D28). To confirm that our model resembles human hindbrain development, we analyzed the expression of several hindbrain and cerebellar markers in our cell line at NES and D28. We first analyzed the expression of *HOXA2* and *OTX1/OTX2* in neural stem cell/progenitor phases in our cell model as the balance of these markers is fundamental for the specification of early hindbrain development (Lowenstein et al., 2022). At D0 and D5, the cells expressed *HOXA2* and not *OTX1/OTX2*, in line with the developing hindbrain phenotype (Fig. S1H). Accordingly, we show that CTRL cells at D28 express many cerebellar markers (*UNC5C, ICMT, CA8, TRPC3, ASTN1, KITLG*) (Aldinger et al., 2021; Consalez et al., 2021; Kim et al., 2003; Kim and Ackerman, 2011; Mancarci et al., 2017; Wu et al., 2019) (Fig. S1I). In parallel, we analyzed cerebellar marker expression in our previously published single-cell RNA-seq (scRNAseq) data from a similarly derived cell line at D28 (Becker et al., 2020) and showed that the cerebellar markers are indeed expressed across the cell types (Fig. S1J). Furthermore, to evaluate the specificity of our model, we analyzed the expression of the markers in a previously published dataset from human cortical organoids (Ressler et al., 2023) and observed extremely low or null expression of the markers in all the cell types and samples (Fig. S1K).

When analyzing the expression of the *HNRNPU* and *HNRNPU-AS1* in the CTRL cell line, we observed that *HNRNPU-AS1* expression decreases from D5 to D28 (comparison D0-D5: P=0.76; D5-D28: P<0.005, ANOVA and post hoc Tukey test), and *HNRNPU* expression decreased steadily during differentiation (comparison D0-D5: P=0.019; D5-D28: P =<1.0×10^{-5}, ANOVA and post hoc Tukey test) (Fig. 1D-E). *HNRNPU* expression follows a similar decreasing trend during differentiation from iPSCs to neurons from a previously published dataset (Burke et al., 2020) and during development of all the cerebral areas, although in the cerebellum the postnatal expression is the highest compared to the other brain regions (Fig. 1G; Fig. S1L). Since *HNRNPU* expression was higher in proliferating progenitor cells (Fig. 1D; Ressler et al., 2023; Sapir et al., 2022), we further inspected its expression in our above mentioned scRNA-seq data (Fig. S2A). As expected, *HNRNPU* expression was highest in the neural progenitor population (Fig. S2B-C). Moreover, the neural progenitor population was further divided into three distinct subclusters, of which one was highly enriched in proliferating markers such as *TOP2A*, *KIFC1,* and *KIF18B*. This cluster also had the highest expression of *HNRNPU* (Fig. S2D).

In contrast to CTRL cells the $HNRNPU_{del/+}$ cells did not show a change in the expression of *HNRNPU-AS1* during differentiation (comparison D0-D5: P=0.92; D5-D28: P =0.84, ANOVA and post hoc Tukey test) (Fig. 1E). Similarly, *HNRNPU* expression was stable from D0 to D5 (P=0.99, ANOVA and post hoc Tukey test), but followed a significantly delayed decrease at D28 (D5-D28, P=2.6×10^{-5}, ANOVA and post hoc Tukey test) (Fig. 1D). In the comparison of RNA expression between CTRL and $HNRNPU_{del/+}$ at each time point, *HNRNPU-AS1* was significantly reduced in $HNRNPU_{del/+}$ at each time point (D0 and D5: P<1.0×10^{-5}; D28: P =0.005, ANOVA and post hoc Tukey test) (Fig. 1E). Instead, at D0 and D5, when the cells express progenitor markers nestin and SOX2 (Fig. S3A), *HNRNPU* expression was significantly lower in $HNRNPU_{del/+}$ cells compared with CTRL cells (P<1.0×10^{-5} and 2.3 x10^{-5}, respectively, ANOVA and post hoc Tukey test), while the expression was similar between the two cell lines at D28 (P=0.58, ANOVA and post hoc Tukey test) (Fig. 1D). HNRNPU protein was predominantly localized in the nucleus at all three analyzed stages of differentiation, and the measured protein levels were extremely variable between different time points in both cell lines and did not mirror mRNA levels (Fig. S3B-C). These results show that physiologically *HNRNPU* has the highest expression in the neuroepithelial stem cell stage and steadily reduces during the differentiation, demonstrating its important role in early neural differentiation.

HNRNPU locus expression impacts cell differentiation pathways

Next, we performed differential gene expression analyses using DESeq2 (Love et al., 2014), followed by gene set enrichment analysis (GSEA) of the obtained transcriptomic data. Similar to earlier reported results in other cell types (Nozawa et al., 2017), we found that *HNRNPU* downregulation had a limited effect on the transcriptional landscape at D0 and D5. The isogenic siHNRNPU cells (replicates n=5) had only 10 differentially expressed genes (DEG) at D0 and 30 DEG at D5 (base mean>20, |log2FoldChange| >0.58, P adjusted<0.05, Wald test and Benjamini-Hochberg procedure) (Table S2A-B). As expected, due to the different genetic backgrounds, when comparing $HNRNPU_{del/+}$ cells (replicates n=5) to the CTRL cell line (replicates n=5) at each time point, we identified a higher number of DEG (2091 DEG at D0 of which 1033 upregulated and 1058 downregulated; 2091 DEG at D5, of which 1251 upregulated and 840 downregulated genes) (Table S2C-D). At D28 of the neural differentiation, both *HNRNPU*-deficient models revealed wider transcriptional rewiring, with 1511 DEG in siHNRNPU and 1608 DEG in $HNRNPU_{del/+}$ cells (Table S2E-F). Of these, only 148 DEG genes were shared between the two models at D28, suggesting that downregulation of *HNRNPU* might affect the expression of upstream transcriptional regulators that increase the transcriptomic landscape variability.

Next, we analyzed gene set and pathway level changes across the two datasets (Table S3). At D0, no specific Gene Ontology (GO) terms or enriched pathways were significantly shared between the two models (Fig. 2A; Fig. S4A, Table S3A-D). At D5, genes affecting the positive regulation of excitatory postsynaptic potential were downregulated in both models. In contrast, among upregulated genes, shared GO terms and enriched pathways included categories referring to the regulation of cell differentiation, growth factor receptors, and constituents of extracellular matrix (Fig. 2A; Fig. S4B, Table S3E-H).

The major transcriptional changes at D28 were clustering in multiple biological processes affected in both $HNRNPU_{del/+}$ and

Biology Open (2023) 12, bio060113. doi:10.1242/bio.060113

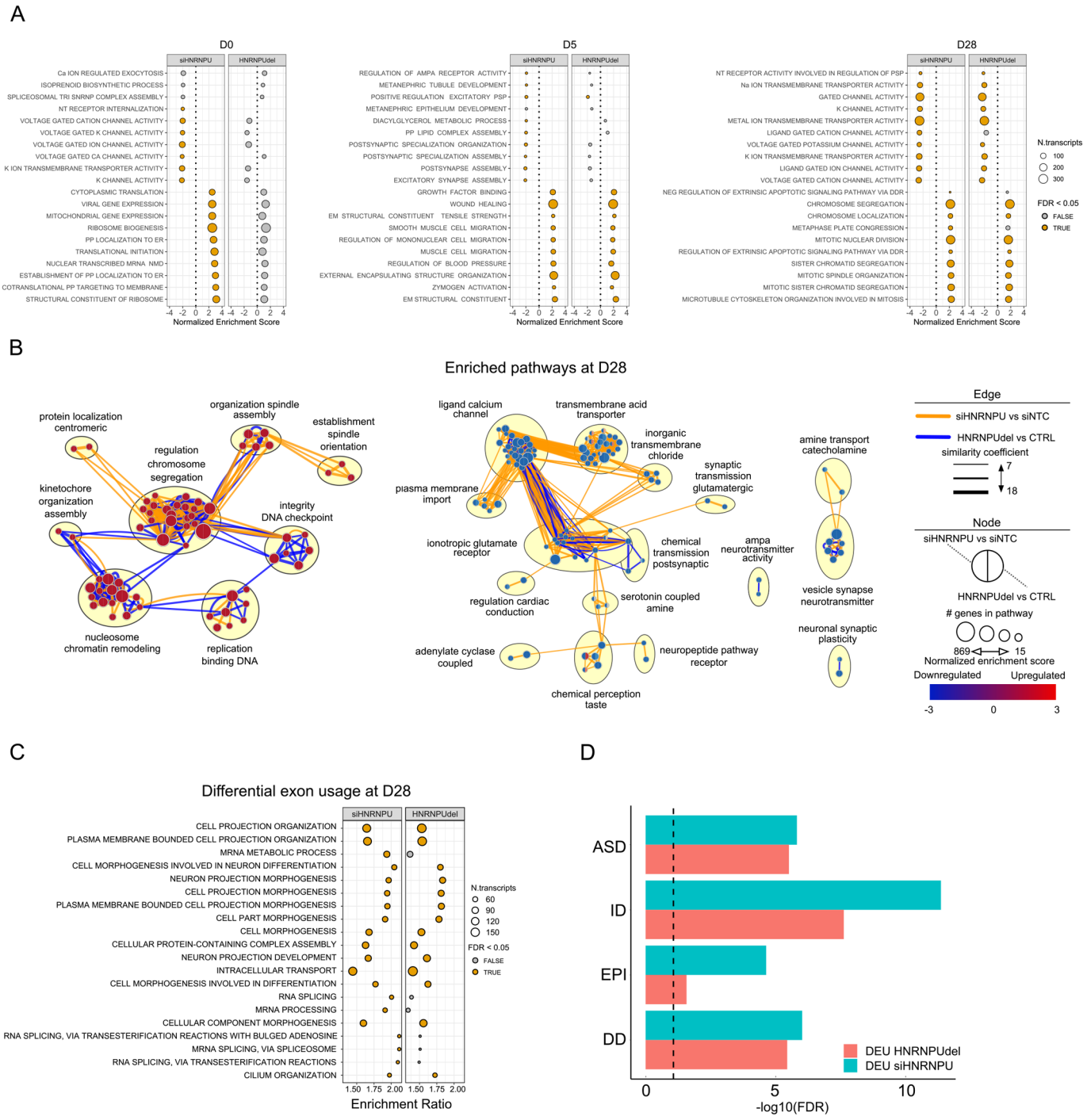

Fig. 2. *HNRNPU* expression affects cell differentiation pathways and modulates exon usage of NDD genes. (A) Top 10 upregulated and downregulated GO terms from ranked differentially expressed genes in siHNRNPU (left panel) and HNRNPU$_{del/+}$ (right panel) at D0, D5, D28. The dotted line marks the limit between the negatively (to the left of the line) and positively (to the right of the line) enriched pathways. ER, endoplasmatic reticulum; NMD, nonsense-mediated decay; PP, protein; NT, neurotransmitter; EM, extracellular matrix; PSP, postsynaptic potential; DDR, death domain receptors; NEG, negative; Na, sodium; K, potassium; Ca, calcium. (B) Selected upregulated (left panel) and downregulated (right panel) pathways enriched at D28. For each node, the left half indicates the enrichment in siHNRNPU versus siNTC, and the right half the enrichment in HNRNPU$_{del/+}$ versus CTRL. The color of the edge indicates which of the datasets significantly contributed to the pathway call (*P* adj <0.05). (C) Top 20 GO terms enriched from genes with differential exon usage in siHNRNPU (left panel) and HNRNPU$_{del/+}$ (right panel) at D28. (D) Enrichment of genes subject to differential exon usage (DEU) in siHNRNPU versus siNTC (cyan) or HNRNPU$_{del/+}$ versus CTRL (magenta) in ASD, ID, epilepsy (EPI), DD gene lists at D28. The vertical dotted line represents the significance threshold of FDR<0.05 (-log10(FDR)>1.3) after hypergeometric analysis. In the figure, the HNRNPU$_{del/+}$ samples are indicated as 'HNRNPUdel'.

siHNRNPU cells. We found 74 significantly enriched GO terms shared between the two models, including several synaptic and transmembrane channel ontologies among the downregulated pathways (Table S3I-L). Interestingly, the shared upregulated pathways from GSEAs included pathways related to cell DNA organization during DNA replication and cell division and more

Biology Open (2023) 12, bio060113. doi:10.1242/bio.060113

general nucleosome and chromatin remodeling pathways (Fig. 2A and B), confirming the role of HNRNPU in the regulation of chromatin organization and DNA replication even in neural cells. Moreover, we found that two key developmental pathways, epithelium tube and embryonic hindlimb morphogenesis, were significantly upregulated in both model systems. Additional dysregulated developmental pathways were also uniquely affected in $HNRNPU_{del/+}$ (Fig. S4C). We also investigated whether the DEG genes at D28 were enriched in genes previously associated with epilepsies, ID, ASD, and general developmental disorders (DD). However, we found no significant enrichment for any gene lists (Hypergeometric test, Table S4). These results suggest that *HNRNPU* deficiency modulates the transcriptomic variability by altering the expression of genes enriched in neural maturation and chromatin organization and mostly affecting cells to be committed to neuronal differentiation more than cells in the neural progenitor phase.

HNRNPU modulates exon usage of NDD genes

Since HNRNPU has previously been shown to affect the transcriptome by regulating alternative splicing (Sapir et al., 2022; Xiao et al., 2012; Ye et al., 2015), we analyzed differential exon usage (DEU), which indicates alternative splicing events or differential isoform usage. Similar to the gene level changes, we detected fewer DEU events (ExonBaseMean >10, |Log2FoldChange| >0.58 and P adjusted<0.05) in the earlier timepoints and more at D28 in both model systems (Fig. S4D and Table S5). When comparing siHNRNPU to siNTC samples, we detected 0 and 2 DEU genes at D0 and D5, respectively, whereas a comparison between $HNRNPU_{del/+}$ and CTRL yielded 35 and 38 DEU genes at D0 and D5, respectively. At D28, 976 and 1285 DEU genes were detected for siHNRNPU and $HNRNPU_{del/+}$ when compared against their respective controls, respectively. Notably, only 5.9% and 9.8% of DEU genes were also differentially expressed in siHNRNPU and $HNRNPU_{del/+}$ cells, respectively. Both models revealed more exclusion than inclusion of exons due to *HNRNPU* deficiency, as 71% of the DEU events were due to downregulation (Fig. S4D). This result is in line with previous findings using other cell types (Huelga et al., 2012; Sapir et al., 2022; Ye et al., 2015). We performed HNRNPU binding motif analysis on differentially used exon (DUE) and flanking intron sequences to evaluate if splicing differences are due to direct binding of HNRNPU. The UGUAUUG binding motif was found on 479 out of 1766 DUEs (padj=1) and 354 out of 1172 DUEs (padj=0.0027) in $HNRNPU_{del/+}$ and siHNRNPU, respectively. In comparison, the motif was present in six of 2946 (padj=0.929) and seven of 2013 (padj=1) flanking introns in $HNRNPU_{del/+}$ and siHNRNPU, respectively. Our results suggests that the DEU observed in HNRNPU deficiency state can be partially caused by the direct binding of HNRNPU. Over representation analysis (ORA) of the DEU genes shared by both models revealed enriched pathways involved in cell morphogenesis, neuron projection development, and cilium organization (Fig. 2C; Table S6). We also analyzed whether DEU genes were enriched for the genes implicated in the different disorders as earlier and found a strong enrichment for ID gene list [hypergeometric test followed with false discovery rate (FDR) correction: 1.49×10^{-14} and 5.26×10^{-10} for siHNRNPU and $HNRNPU_{del/+}$, respectively], ASD (8.26×10^{-8} and 1.96×10^{-7}), DD (4.68×10^{-8} and 2.36×10^{-7}), and epilepsy (2.28×10^{-6} and 0.012) (Fig. 2D; Table S4). Our results are in line with earlier evidence and showcase the role of HNRNPU in regulating exon usage during neural development, of genes previously associated with several NDDs.

HNRNPU locus deficiency increases the proportion of neural progenitor cells during differentiation

Transcriptional changes at the pathway level strongly indicated differences in the cell proliferation rate of $HNRNPU_{del/+}$ and siHNRNPU cells at D28; therefore, we focused on analyzing the neural progenitor pool at D28, a timepoint in which generally most of the cells are postmitotic and committed for neuronal differentiation. First, we analyzed the cell type proportions using deconvolution of the transcriptomic data similar to previously described (Becker et al., 2020). The deconvolution predicted a higher proportion of neural progenitors in $HNRNPU_{del/+}$ compared to CTRL (Fig. 3A; Fig. S5A). To validate the presence of neural progenitors across the differentiation and investigate the difference between the two models, we analyzed SOX2 positive nuclei at the three time points for both $HNRNPU_{del/+}$ and CTRL cell lines. As expected, each cell line showed a decreasing number of SOX2-positive cells during the differentiation time course. However, $HNRNPU_{del/+}$ cells displayed a significantly higher number of SOX2-positive cells at D5 and D28 compared to CTRL ($P<10^{-4}$ and 0.002, respectively, χ^2 test) (Fig. 3B; Fig. S5B). Also, the siHNRNPU model had an increased number of SOX2-positive cells at D28, but the difference was insignificant ($P=0.16$, χ^2 test) compared with siNTC cells (Fig. 3B). To evaluate the characteristics of the progenitor cells at D28, we measured cell proliferation by Bromo-deoxy-uridine (BrdU) incorporation in both conditions. As expected, the cell proliferation rate decreased throughout the differentiation and was significantly higher in both siHNRNPU and $HNRNPU_{del/+}$ cells at D28 compared to the relative controls at the same time point ($P=0.002$ and 0.01, respectively, two-sided *t*-test). The rate was similar between $HNRNPU_{del/+}$ and CTRL cell lines at D0 but diverged already at D5 ($P=6\times10^{-3}$, two-sided *t*-test) (Fig. 3C; Fig. S5C). In summary, downregulation of the HNRNPU locus leads to an enrichment of proliferating neural progenitor cells in the mixed population at D28 compared to controls. This suggests either a delay in the maturation trajectory during differentiation or a reduced proportion of cells committing to differentiation.

HNRNPU locus downregulation alters the maturation of neural cells

Since the dysregulated pathways in both *HNRNPU*-deficient conditions were related to membrane channels, synaptic formation, and extracellular matrix, we hypothesized that *HNRNPU* deficiency could affect the stage of neuronal maturation. To validate this hypothesis and the transcriptomic results, we first analyzed the proportion of cells with primary cilia during neural differentiation, as primary cilia guide axon tract development (Guo et al., 2019). Additionally, our results for DEU genes showed the enrichment of cilium organization in siHNRNPU and HNRNPUdel/+ cells at D28. Therefore, we analyzed ciliary proteins ARL13 and PCNT expression by immunofluorescence in CTRL and $HNRNPU_{del/+}$ cells throughout differentiation and observed a higher number of ciliated cells at D5 compared to D0 in both cell lines and no difference between *HNRNPU* deficiency and control cells at D0 and D5 ($P=0.37$ and $P=0.64$, respectively, χ^2-test). However, a significant difference in the proportion of ciliated cells was observed at D28 ($P=1.497\times10^{-6}$, χ^2-test), wherein $HNRNPU_{del/+}$ cells had a higher percentage of ciliated cells (Fig. 3D). Since the alteration of cilium organization pathways was similarly significant in both experimental conditions, we considered sufficient to validate the finding by immunofluorescence only in the $HNRNPU_{del/+}$ condition.

Additionally, we analyzed the expression of the presynaptic marker Synapsin 1/2 and the postsynaptic marker Homer1. The

Biology Open (2023) 12, bio060113. doi:10.1242/bio.060113

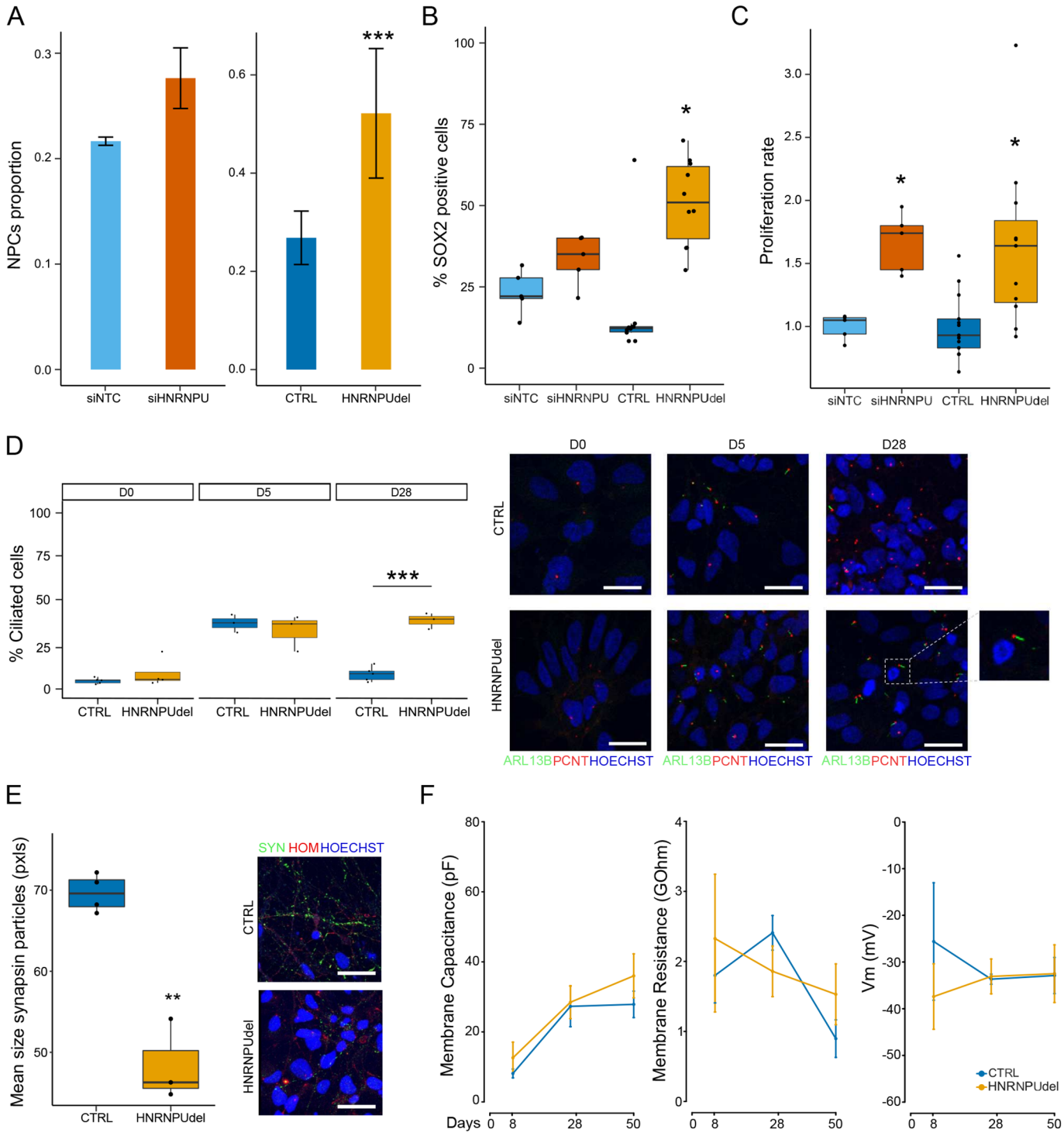

Fig. 3. Cells at the late-differentiation stage show higher progenitor phenotype and affected synaptogenesis under *HNRNPU* downregulation. (A) Neural progenitor cells proportion in siNTC, siHNRNPU, CTRL, HNRNPU$_{del/+}$ at D28 estimated by deconvolution analysis. (B) Percentage of cells positive at the staining with SOX2 antibody at D28. (C) Proliferation rate of siNTC, siHNRNPU, CTRL, HNRNPU$_{del/+}$ at D28. (D) Immunofluorescence of primary cilia with ciliary marker ARL13B and basal body marker PCNT in CTRL and HNRNPU$_{del/+}$ and quantification of ciliated cell proportions. Pictures were acquired with 63× magnification, 0.5 zoom and z-stack. Scale bar: 20 µm. (E) Immunofluorescence of synapsin 1/2 in CTRL and HNRNPU$_{del/+}$ at D28 and quantification of the mean size of the synapse particles positive to synapsin 1/2 staining. Pictures were acquired with 63× magnification and z-stack. Scale bar: 20 µm. (F) Electric properties of the membrane of CTRL and HNRNPU$_{del/+}$ cells at different time points. *P<0.05, **P<0.001, ***P<0.0001. In the figure HNRNPU$_{del/+}$ samples are indicated as "HNRNPUdel".

HNRNPU$_{del/+}$ cells had significantly smaller presynaptic particle sizes than the CTRL cells (P=0.009, t-test, two-sided) (Fig. 3E). In contrast, the number of presynaptic particles and the number and size of postsynaptic signals were comparable between HNRNPU$_{del/+}$ and CTRL. To monitor the neuronal maturation, we performed patch clamp electrophysiology to study the intrinsic membrane properties

Biology Open (2023) 12, bio060113. doi:10.1242/bio.060113

and synaptic activity of HNRNPU$_{del/+}$ and CTRL cells at D8 (n=4), D28 (n=12 cells for CTRL, and 17 cells for HNRNPU$_{del/+}$), and D50 (n=7 cells for CTRL and 10 cells for HNRNPU$_{del/+}$) (Fig. 3F). However, despite the clear neuronal morphology (Fig. S5D), the cells were characterized by high membrane resistance in response to voltage-step commands, and no spontaneous excitatory or inhibitory synaptic currents could be measured in any of the recorded cells, therefore at this stage of differentiation neither CTRL nor HNRNPU$_{del/+}$ cells can be considered mature neurons.

HNRNPU locus downregulation affects nuclear shape and chromatin organization

The results of our transcriptional profiling revealed a role of HNRNPU in chromatin organization, in line with previous reports that demonstrated the function of HNRNPU in chromatin compaction, DNA synthesis, and chromosome folding during mitosis in different cell types and conditions (Connolly et al., 2022; Nozawa et al., 2017; Sharp et al., 2020). Therefore, we sought to investigate whether *HNRNPU* deficiency affects chromatin organization in our human neural cell model. First, we performed chromatin accessibility analyses by treating CTRL and HNRNPU$_{del/+}$ cells with DNaseI; however, no large-scale differences were visible (Fig. S6A). We then performed single-cell immunofluorescent analysis of cell nuclei stained for heterochromatin marker, histone 3 tri-methylation at lysine 9 (H3K9me3). Both *HNRNPU*-deficient cell models displayed profound changes in nuclear architecture at D28 (Fig. 4A). Specifically, upon *HNRNPU* deficiency, a subpopulation of cells displayed differential number and total volume of heterochromatic foci (NbF, VFTotal, respectively), intensity and volume of the relative heterochromatic fraction (Intensity RHF, Volume RHF), and nuclear shape characteristics like surface area, volume, and radius of a sphere of equivalent volume (ESR) (Fig. 4A).

Chromatin rewiring upon *HNRNPU* locus downregulation

Next, we performed Hi-C to investigate the changes in chromatin organization at a higher resolution (Lieberman-Aiden et al., 2009). Since the NucleusJ analyses showed similar alterations of the heterochromatic fraction and nuclear shape in the two experimental conditions, we performed HiC on CTRL and HNRNPU$_{del/+}$ cells at D0 and D28 (Fig. S6B-C; Materials and Methods) as a model for HNRNPU haploinsufficiency. The number of chromatin interactions throughout the genome was similar at D0 between the two cell lines. However, at D28, a diverging pattern appeared in the chromatin organization maps, with the largest differences observed at the level of A/B compartments (10^5–10^6 base pairs) (Fig. S6D). Furthermore, while the ratio of short and long-range contacts per chromosome was similar at D0, at D28 CTRL cells showed a higher ratio for the short- and long-range contacts than HNRNPU$_{del/+}$ cells (Fig. S6E). An analysis of differential chromosome contact frequencies between the HNRNPU$_{del/+}$ and CTRL cells revealed little differences at D0 and higher contact differences at D28, as shown by the log2 ratio of the contacts at the chromosome level (Fig. 4B).

Furthermore, a compartment interaction analysis revealed similar interaction strengths between the samples at D0 (compartmentalization strength: 1.30 and 1.28 for CTRL and HNRNPU$_{del/+}$ cells, respectively). In contrast, we observed stronger compartmentalization in HNRNPU$_{del/+}$ at D28 (1.31 versus 1.59 for CTRL and HNRNPU$_{del/+}$ cells, respectively), with higher interactions between active compartments (A compartment) and fewer trans-interactions compared to the CTRL cells (Fig. 4C). These results align with the Hi-C experiments previously conducted on *Hnrnpu*-deficient mouse hepatocytes, showing decreased A-B interactions and increased A-A and B-B interactions upon *Hnrnpu* downregulation (Fan et al., 2018).

Next, we analyzed the compartment composition of each sample to identify genomic regions that switch compartments between CTRL and HNRNPU$_{del/+}$ (Materials and Methods). At D0, 3% of the compartments switched from inactive (B) to active (A) compartment and 5.6% from A to B comparing CTRL and HNRNPU$_{del/+}$, while at D28, 4.2% switched from B to A and 8.6% from A to B (Fig. 4D). To investigate whether these compartment switches affect disorder-related genes, we assessed the enrichment for the genes mapping in genomic regions that switch compartments. Genes mapped in regions switching from A to B compartment were enriched in all the gene lists (ASD FDR: 0.0043; ID: 0.0018; epilepsy: 0.0035, DD: 0.0136; hypergeometric test), whereas genes mapping in regions switching from B to A compartment were enriched only in the ASD gene list (FDR=0.0136) (Fig. 4E and Table S4). In contrast, we found no significantly enriched GO terms.

Lastly, we investigated whether the compartment changes were related to the transcriptional changes described above. Therefore, we mapped the DEGs at D28 (|log2FC|> 0.58, base mean>20) with gene mapping in the switching compartments. The concordant genes were defined as genes mapping to a region with a compartment switching from A to B and downregulated in the transcriptome analysis, or genes mapping in the B to A compartment switch and upregulated. We identified 144 concordant genes at D0 and 241 concordant genes at D28 (Table S7). Only concordant genes mapping in the compartment switching from A to B at D28 were significantly enriched for ASD (FDR: 0.014) and epilepsy (FDR: 0.007) gene lists (Fig. 4E; Table S4). By further analyzing the concordant genes to identify the enriched pathways, we showed that no ontologies were enriched in the concordant B to A genes, while the most significant enriched GO term in the concordant A to B genes was ‘GABA-gated chloride ion channel activity’ (FDR<0.05) (Fig. S6F), driven by genes such as *CACNB2*, *GABRA2*, *GABRA4*, *GABRB1*, *GABRG1,* and *SCN1A*. Interestingly, the *GABR* family genes downregulated in HNRNPU$_{del/+}$ at D28 belong to a cluster on chromosome 4 with an approximately seven megabase (Mb) region that maps in the A compartment in CTRL and B compartment in HNRNPU$_{del/+}$ at D28 (Fig. 4F).

Overall, the Hi-C analysis showed that, similar to the transcriptome analyses, the compartment organization is more affected in HNRNPU$_{del/+}$ at D28 than at D0, and *HNRNPU* deficiency led to an enrichment of B compartments at both timepoints. Interestingly, genes mapping in the enriched B compartments are associated with ASD and epilepsy, suggesting that the chromatin remodeling dependent on HNRNPU expression might ultimately be the driver of the observed phenotypes.

DISCUSSION

Heterozygous genetic variants in the *HNRNPU* locus lead to various disorders with predominant brain phenotypes. Recently, few studies focused on the effects of mutations in *HNRNPU* gene in mouse and human cortical organoids. Here, we model microdeletions of the *HNRNPU* locus responsible of HNRNPU-related disorder and provide novel evidence of the molecular and cellular consequences of *HNRNPU* deficiency in differentiating human neuronal cells with hindbrain phenotype, adding knowledge on the effect *HNRNPU* deficiency on the brain region where *HNRNPU* expression is the highest.

Biology Open (2023) 12, bio060113. doi:10.1242/bio.060113

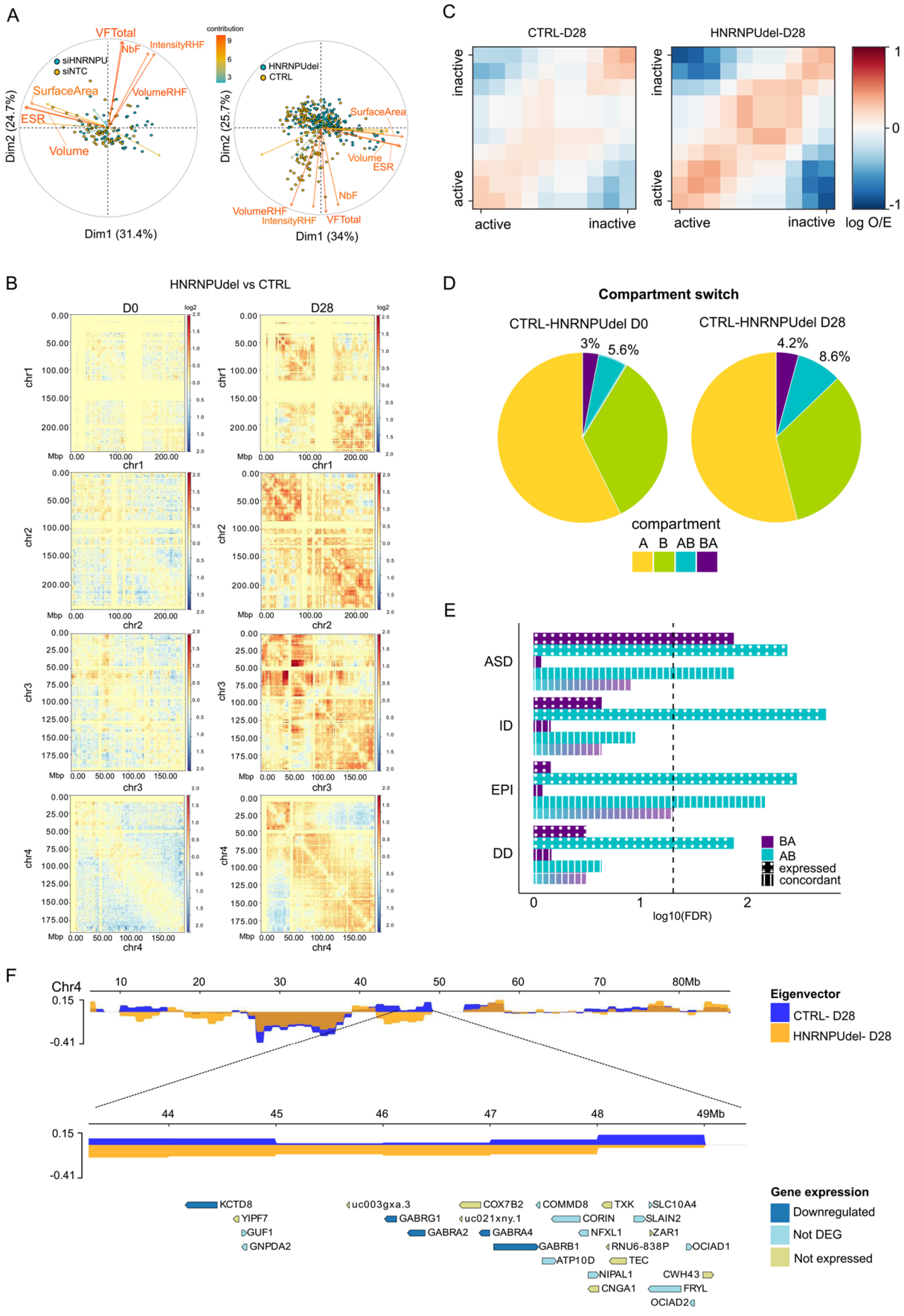

Fig. 4. See next page for legend.

Biology Open (2023) 12, bio060113. doi:10.1242/bio.060113

Fig. 4. *HNRNPU* downregulation affects chromatin organization. (A) Biplot of the contribution of the variables generated by NucleusJ for the clustering of the nuclei after H3K9me3 staining, compared siHNRNPU with siNTC (left panel) and $HNRNPU_{del/+}$ with CTRL (right panel). (B) Example of normalized log2ratio of the contacts for each chromosome of $HNRNPU_{del/+}$ compared with CTRL, at D0 and D28, after ICE correction. (C) Saddle plot of the *cis*- and *trans*- interactions of the A (active) and B (inactive) compartments in CTRL and $HNRNPU_{del/+}$ at D28. (D) Genome-wise compartment switch at D0 and D28 in the comparison for each time point of $HNRNPU_{del/+}$ and CTRL. (E) An enrichment of genes within the compartment switch regions in ASD, ID, epilepsy (EPI), and DD gene lists at D28. 'Expressed', indicated by the dotted pattern, include genes that map in one of the compartment switches and are expressed in our dataset (gene count >20 in at least one sample). 'Concordant', indicated by the vertical lines pattern, includes the genes that are upregulated from the transcriptome analysis and map in a compartment B in CTRL and A in $HNRNPU_{del/+}$ or vice versa. The vertical dotted black line represents the significance threshold of FDR<0.05 (-log10(FDR)>1.3) after the hypergeometric test corrected for all the comparisons. (F) Representative compartment switch from A to B at D28 between CTRL and $HNRNPU_{del/+}$ on chromosome 4 (chr4). The upper panel shows the eigenvectors of the first 90 Mb of chr4 for each sample (yellow for $HNRNPU_{del/+}$ and blue for CTRL). The zoom-in panel shows the eigenvectors of the two samples in the chromosome location of chr4: 43-49 Mb. The lowest panel shows the genes mapping onto the switch region (dark blue: downregulated genes in the $HNRNPU_{del/+}$ -CTRL comparison; light blue: expressed in the dataset but not differentially expressed in the two conditions; light green: not expressed). In the figure $HNRNPU_{del/+}$ samples are indicated as 'HNRNPUdel'.

We demonstrate that adequate levels of transcripts from the *HNRNPU* locus are needed in the early developmental transition from neural progenitors to developing neurons for proper neurogenesis. Our results, consistent with the earlier reports, show that *HNRNPU* expression is highest at early neural stem cell and progenitor stages and in a subpopulation of neural progenitors at the later stage of neuronal differentiation (Connolly et al., 2022; Sapir et al., 2022). Despite this high expression, results indicate that *HNRNPU* deficiency does not affect neural cells at this early stage.

In contrast, as the neural progenitor cells commit to differentiation, the reduced *HNRNPU* levels led to a higher number of dividing neural progenitors compared to the control stage, in a phase where the proportion of progenitor cells should decrease. This delayed transition from progenitors to differentiating neurons could explain the lack of differences in *HNRNPU* expression in $HNRNPU_{dcl/+}$ from D0 and D5, and the almost equal expression levels with CTRL cells at D28, despite the heterozygous deletion of one allele. A recent study showed opposite effects for the complete loss of *Hnrnpu,* as it led to decreased proliferation followed by cell death of neural progenitors and postmitotic neurons in mice (Sapir et al., 2022). As heterozygous mutations in *HNRNPU* are not lethal, and the severity of the phenotypes in *HNRNPU*-related disorders is variable (Balasubramanian, 2022), embryonic cells can likely adapt to low levels of *HNRNPU* and still proliferate and differentiate. Therefore, it is reasonable that iPSCs and NES cells that retain 30–70% of the physiologic *HNRNPU* levels do not show a major phenotype, as we have shown here. Instead, we propose that cells with *HNRNPU* haploinsufficiency are inadequate to drive efficient cell fate transition of mitotic cells int differentiating neurons and other neural cells through multiple regulatory pathways, leading to stochastic rewiring of the hindbrain development. Indeed, altered regulation of proliferation has been demonstrated to cause defects in the progenitors' fate and, ultimately, neuronal development trajectories (Lalli et al., 2020; Pilaz et al., 2016). In several cellular models of ASD, unbalanced neural progenitors population due to both hyper- and hypo-proliferation of the progenitors have been documented (Connacher et al., 2022; Marchetto et al., 2017; Mowat et al., 2003; Zucco et al., 2018). Accordingly, we hypothesize that the observed downregulation of the synaptic and neuronal maturation markers is due to abnormal enrichment of progenitors at D28 stage and a consequence of the delayed maturation process. This observation is in contrast with what was observed in a recently published study on human cortical organoids, where *HNRNPU* mutations are shown to associate with downregulation of ontologies referring to nucleic acid binding and upregulation of neurogenic pathways (Ressler et al., 2023). The dysregulated genes are partially resembling transcriptomic alterations in embryonic mice carrying a heterozygous mutation in *HNRNPU* but are discordant with the perinatal mice. Thus, the stage of cell maturation and development in which the analyses are performed seem to be critical for studying effects of HNRNPU. Moreover, in this study, we are modeling the effect of the microdeletion of the whole *HNRNPU* locus on a hindbrain cell model, in contrast with single *HNRNPU* mutations on brain cortex systems, likely contributing to the discrepancy of the observed effects of *HNRNPU* mutations.

We provide mechanistic insights that both RNA processing and chromatin regulation in early brain development play a critical role in the observed brain phenotypes in *HNRNPU*-related disorders. It has been earlier demonstrated that the correct pool of mRNA isoforms from the alternative splicing process is important in the transition from progenitor cells to neurons in the developing cerebral cortex (Zhang et al., 2016), and RNA splicing is one of the key enriched pathways from molecular and genetic studies of ASD (Gandal et al., 2018; Satterstrom et al., 2020). Therefore, our and others' results pinpoint that further delineation of the RNA splicing program during the early steps of brain development is essential for understanding the origins of NDDs.

Furthermore, the importance of 3D genome organization for cell fate decisions during neural development is starting to emerge, showing that dynamic changes at multiple levels of chromatin organization are needed for these processes (Bonev et al., 2017; Hu et al., 2021). This is in line with our results showing major reorganizations in a later stage of neural differentiation. Indeed, multiple NDD cell models have shown that the dysfunction of the chromatin organization leads to changed neuronal maturation (Calzari et al., 2020; Markenscoff-Papadimitriou et al., 2021; Parisian et al., 2020; Su et al., 2021).

We additionally provide evidence of cellular processes, such as cilia organization and initial synaptogenesis, that are affected by the molecular changes in the *HNRNPU* deficiency state. For instance, we demonstrate an increase in ciliated cells. Recently, HNRNPU was indicated to localize occasionally to cilium in mice brain cells (Sapir et al., 2022). As *HNRNPU*-related disorders share many phenotypic features with ciliopathies (Balasubramanian, 2022; Focșa et al., 2021), the connection between cilia organization and *HNRNPU* warrants more studies.

In conclusion, we present the first suggestive evidence that *HNRNPU* mutations in human hindbrain neural progenitors result in inadequate transition to commitment to neurogenesis. This, in turn, leads to large-scale effects on chromatin organization and transcriptional landscape at later stages of neural development and presumably to diverging trajectories of neurons and other neural cells. Follow-up studies of direct targets, different developmental stages, and brain regions using both two-dimensional (2D) and organoid models will be needed to assess better the impact of *HNRNPU* haploinsufficiency on neurogenesis and its role in the pathogenesis of *HNRNPU*-related disorders.

Limitations of the study

We acknowledge that this study has limitations, including that we only compare the isogenic model constructed with siRNA with one

Biology Open (2023) 12, bio060113. doi:10.1242/bio.060113

Table 1. Key resources

Reagent or resource	Source	Identifier
Chemicals, peptides, and recombinant proteins		
DMEM/F-12 Glutamax	ThermoFisher Scientific	31331-093
Penicillin/ Streptomycin	ThermoFisher Scientific	15140122
Laminin from Engelbrecht-holm-swarm murine cells	Sigma-Aldrich	L2020
B-27 Supplement	ThermoFisher Scientific	17504044
N-2 Supplement	ThermoFisher Scientific	17502001
Poly-L-ornithine	Sigma-Aldrich	P3655
Bovine serum albumin	Sigma-Aldrich	A7030
DNase I	ThermoFisher Scientific	EN0521
Accell SMARTpoolcsbarline si-HNRNPU	Dharmacon	E-013501-00-0010
Accell SMARTpoolcsbarline si-NTC	Dharmacon	D-001950-01-20
Neural isolation enzyme	ThermoFisher Scientific	88285
TrypLE express	Gibco	12604013
Diamond antifade mountant	ThermoFisher Scientific	15205739
Anti-H3K9me3 antibody	Abcam	Ab6000
Anti-Nestin antibody	Merck-Millipore	MAB5326-KC
Anti-SOX2 antibody	Merck-Millipore	AB5603
Anti-HNRNPU antibody	Novus Biologicals	NBP2-49290
Anti-MAP2 antibody	Merck-Millipore	M2320
Anti-SYNAPSIN1/2 antibody	Synaptic System	106006
Anti-HOMER1 antibody	Synaptic System	160011
Anti-ARL13B antibody	Proteintech	17711-1-AP
Anti-PCNT antibody	Abcam	Ab28144
Anti-mouse AlexaFluor488	Invitrogen	A21202
Anti-rabbit AlexaFluor555	Invitrogen	A31572
Anti-chicken AlexaFluor488	Jackson Immuno research	703-545-155
Anti-mouse CF555	Biotium	20037
Critical commercial assays		
Arima-HiC kit	Arima Genomics	A510008
BrdU assay	Abcam	ab126556
ReliaPrep RNA Miniprep	Promega	Z6012
Total Protein Detection Module for Jess, Wes, Peggy Sue, or Sally Sue	Biotechne	DM-TP01
EZ Standard pack WES	Biotechne	PS-ST01EZ-8
Deposited data		
RNA-seq and HiC analysis pipeline	GitHub	https://github.com/Tammimies-Lab/HNRNPUdeficiency-Mastropasqua-et-al.
Bulk RNA-seq	NCBI GEO	GSE229004
HiC	ENA	*Pending*
Software and algorithms		
R (v4.1.2)	R	r-project.org
DESeq2 (v1.34)	Bioconductor	10.18129/B9.bioc.DESeq2
Cytoscape (v3.9.0)	Cytoscape	cytoscape.org
EnrichmentMap (v3.3.3)	Cytoscape	10.1371/journal.pone.0013984
GSEA (v4.2.1)	Broad Institutet	10.1073/pnas.0506580102
AutoAnnotate (v1.3.5)	Cytoscape	10.12688/f1000research.9090.1
ggplot2 (v3.3.5)	CRAN	ggplot2.tidyverse.org
DEXSeq (v1.40)	Bioconductor	10.18129/B9.bioc.DEXSeq
HiCExplorer (v 3.7)	HiCExplorer	10.1038/s41467-017-02525-w
FanC (v 0.9.2)	FanC	10.1186/s13059-020-02215-9
WebGestaltR (v0.4.4)	CRAN	https://doi.org/10.1093/nar/gkz401

patient cell line, providing the limited possibility to analyze the genetic background effects, recently shown to be highly important to study (Paulsen et al., 2020 preprint). Moreover, while mimicking the heterozygous deletion of the whole locus, we cannot distinguish if the observed effects are mainly driven by HNRNPU or if they are the results of a combined role of HNRNPU and *HNRNPU-AS1*. Furthermore, we focused on a very early model of neural development using NES cells and undirected differentiation, which cannot represent the complexity of the human hindbrain. The analyses described here are from a pool of cells not sorted for the cell type or analyzed as single cells, thus, we only give a general overview of the transcriptional and chromatin organization landscape related to *HNRNPU* haploinsufficiency. Further studies using single-cell techniques, different neuronal differentiation models and hindbrain human organoids should be employed to present the cell-specific effects of *HNRNPU* mutations in later stages of brain development.

MATERIALS AND METHODS

Identification of the individuals with *HNRNPU* deletion and phenotypic characterization

We have earlier performed a screening for copy number variation in a twin sample from The Roots of Autism and ADHD study in Sweden (RATSS) (Bölte et al., 2014; Stamouli et al., 2018) in which we identified a male twin

Biology Open (2023) 12, bio060113. doi:10.1242/bio.060113

pair carrying the deletion on chr1:244997953-245042312 (hg19) encompassing *HNRNPU*. The twin pair has undergone an extensive phenotypic characterization, including evaluation for ASD, ID, and other NDDs, cognitive testing, and medical examination (Table S1). Written informed consent was obtained from individuals and their parents prior to the study. The study was approved by the regional and national ethical boards in Sweden and has been conducted in accordance with the Declaration of Helsinki for medical research involving human subjects, including research on identifiable human material and data.

Cell culture

Human iPSC cells were derived from fibroblasts of one of the twins from the RATSS study, a male carrying a 44Kb mutation of the HNRNPU locus spanning through *COX20*, *AS1-HNRNPU,* and *HNRNPU*, using a previously described protocol (Uhlin et al., 2017b). Human iPSC cells were cultured in mTeSR Plus (Stem Cell Technology) on 5 µg/ml BioLaminin 521LN (Biolamina) precoated vessels. Pluripotency and normal karyotype were confirmed, as shown in Fig. S1. Dual-SMAD inhibition was applied to derive neuroepithelial stem (NES) cells from human iPS cells as described previously (Chambers et al., 2009; Falk et al., 2012). Patient-derived and previously established NES cells from a male neurotypical donor (Uhlin et al., 2017a) were seeded on 20 µg/ml poly-L-ornithine (Sigma Aldrich), and 1 µg/ml laminin (Sigma Aldrich) precoated plastic surfaces in DMEM/F12+Glutamax medium (Gibco) supplemented with 0.05X B-27 (Gibco), 1× N-2 (Gibco), 10 ng/ml bFGF (Life Technologies), 10 ng/ml EGF (PeproTech) and 10 U/ml penicillin/streptomycin (Gibco), replacing media every day. For immunofluorescence, the glass coverslips were precoated with increased concentrations of poly-L-ornithine to 100 µg/ml and laminin to 2 µg/ml. Cells were maintained in a 5% CO_2 atmosphere at 37°C. Upon starting the differentiation, cells were changed to medium with an increased 0.5× B-27 concentration without bFGF and EGF. Two-thirds of media supplemented with 0.4 ug/ml laminin was changed every other day until differentiation 15; whereafter media was changed every third day. NES cells were harvested two days after culturing and neural cells were harvested after 5, 28 or 50 days of differentiation.

DNAse I sensitivity assay

Cells were grown and harvested as earlier described and resuspended in cold RSB buffer: 10 mM Tris-HCl (pH7,4), 10 mM NaCl, and 3 mM $MgCl_2$. Cells were then lysed in cold lysis buffer (RSB buffer and 0,2% Triton X-100) and centrifuged to collect nuclei in the pellet. The nuclei were then incubated with different amounts of DNase I enzyme (0, 1, 3, 5, 0, 15 units) at 37°C for 10 min. The digestion was blocked by adding 50 mM of EDTA followed by incubation at 55°C for 1 min. The results of the digestion were visualized on an 0.8% agarose gel.

siRNA-mediated silencing

Cells were transfected with 0.5 µM Accell SMARTpool siRNA targeting *HNRNPU* mRNA (Dharmacon E-013501-00-0010) or 0.5 µM Accell Nontargeting siRNA (Dharmacon D-001950-01-20) according to manufacturer's protocol. The siRNA pool consisted of the following oligos: oligo1: UCUUGAUACUUAUAAUUGU, oligo2: CUCGUAUGCUAAGAAUGGA, oligo3: GUUUCAGGUUUUGAUGCUA, oligo4: CUAGUGUGCUUGUAGUAGU. NES cells were transfected one day after seeding, and samples were collected 24 h after treatment. Cells under differentiation were transfected once in the NES phase, once when changing media to differentiation media, and thereafter every sixth day until D28 sample harvesting.

Immunofluorescence and image analysis

Cells on glass coverslips were fixed in 4% formaldehyde for 20 min at room temperature and washed with 1× TBS. Blocking was performed with 5% Donkey Serum and 0.1% Triton X-100 in 1× TBS for 1 h. Primary antibodies diluted in blocking buffer (Nestin 1:1000; SOX2 1:1000; Synapsin 1/2 1:500; Homer1 1:250; MAP2 1:500; HNRNPU 1:500; H3K9me3 1:500, ARL13B 1:10,000, PCNT 1:250) were incubated at +4°C overnight. Careful washing was done with 1× TBS, and secondary antibodies diluted 1:1000 in blocking buffer were incubated at room temperature for 1 h, covered from light. Coverslips were washed and mounted with Diamond Antifade Mountant (ThermoFisher Scientific). Images were acquired with LSM 700 Zeiss Confocal Microscope using 20× or 63× magnification and 0.5 µm z-stack through the sample.

At least three replicates per sample were stained and analyzed for the immunocytochemistry analyses. The images stained with synapsin 1/2 were analyzed with ImageJ plugin Synapse Counter, and the statistical Student's *t*-test analyses were performed in R. The statistical analyses for SOX2 positive nuclei were performed in R by χ^2-test. For primary cilia analysis, a cell was considered ciliated if positive for both cilia markers ARL13B and PCNT; the statistical testing was performed in R by χ^2-test. For the images of the nuclei stained with the H3K9me3 antibody, the single nuclei were cropped using an in-house built macro for ImageJ. A minimum of thirty nuclei per replicate was analyzed with NucleusJ, a plugin of ImageJ, using the default settings (Poulet et al., 2015).

Capillary Western blot

Cells were collected in extraction buffer (50 mM Tris-HCl, 100 mM NaCl, 5 mM EDTA, 1 mM EGTA) supplemented with a 1× protease inhibitor cocktail (ThermoFisher Scientific) using a plastic cell scraper. The samples were sonicated with six short pulses at 36% amplitude (Vibra-Cell VCX-600, Sonics). Protein concentrations were measured with Qubit Protein Assay Kit (ThermoFisher Scientific). The total protein sample (150 ng/µl) was loaded on the capillary Western blot system Simple-Western-JESS (Bio Techne), multiplexed for total protein and chemiluminescence detection of HNRNPU (1:10 dilution). Data were analyzed using Compass for S.W. software (5.0.1), and the HNRNPU peak area was normalized against the total protein area. Three to five biological replicates were analyzed for each time point, and the significance at each time point was evaluated by Student's *t*-test.

RNA extraction and bulk RNA sequencing analyses

Cells were lysed in TRIzol reagent (Invitrogen), and RNA isolated with ReliaPrep RNA Cell Miniprep kit (Promega Z6012). We extracted RNA samples for three to five biological replicates per cell line and time point. Samples were delivered to NGI Sweden for library preparation and sequencing. The samples were subjected to library preparation with Illumina Truseq Stranded total RNA RiboZero GOLD kit, except for siNTC-D28 and siHNRNPU-D28 libraries prepared with Illumina TruSeq Stranded mRNA kit due to low RNA yields. All libraries were sequenced on the NovaSeq6000 platform with a 2×151 setup using NovaSeqXp workflow in S4 mode flowcell. We obtained, on average, 35 and 65 million reads per sample for early time points and D28, respectively, with a minimum 82,7% alignment rate.

Differential gene expression analysis was performed using DESeq2 (v1.24.0) (Love et al., 2014) in R (v4.1.2). The significance thresholds used were adjusted P value<0.05 (Benjamini-Hochberg adjustment), base mean >20, and absolute log2 fold change >0.58. Pathway analysis was done according to previously described protocols (Reimand et al., 2019). In short, the ranked gene expression list was used in gene set enrichment analysis (GSEA) (Version 4.3.0) to analyze the enrichment in the gene ontology, molecular function, and biological process gene lists (v. 7.4), and enriched categories were visualized in Cytoscape (v3.8.2) with Enrichment Map (v3.1.0) and AutoAnnotate (Merico et al., 2010; Reimand et al., 2019; Shannon et al., 2003).

Differential exon usage analysis was performed using the DEXSeq package (v1.40.0) (Anders et al., 2012). A flattened annotation file was created using provided python script, excluding the aggregate exon bins, and exon counts were counted using provided python script. The analysis was performed with the formula ~ *sample+exon+condition: exon.* A gene was called to have evidence for DEU if at least one exon bin was differentially used between conditions. The difference was considered significant with FDR (Benjamini-Hochberg adjustment) adjusted P<0.05, exon base mean >10, and an absolute log2 fold change>0.58. Over-representation analysis (ORA) was performed using the online tool WebGestalt (Liao et al., 2019). In addition, hypergeometric tests were used to test for enrichment between differentially expressed genes and DEU genes and specific NDD-related

Biology Open (2023) 12, bio060113. doi:10.1242/bio.060113

gene lists: ASD gene list (SFARI genes selected for score 1,2 and syndromic, release 07-20-2022), ID gene list (green and amber genes from https://panelapp.genomicsengland.co.uk/ v3.1632), epilepsy gene list (green and amber genes from https://panelapp.genomicsengland.co.uk/ v2.547) and general development [compiled gene list (Becker et al., 2020)].

HNRNPU binding motif analysis was performed using AME function (McLeay and Bailey, 2010) of MEME-Suite v5.5.3 with default settings and background datasets of all expressed exons with exon base mean >10 (151878 and 150565 exons) and their flanking introns (156090 and 159915) in HNRNPUdel and siHNRNPU. The position weight matrix for UGUAUUG motif was downloaded from RBPmap. The exon bins obtained from DEXSeq were collapsed with annotated exons using Intersect function of Bedtools v2.31.1. In instances of overlapping exons, the longest exon was selected for the analysis. The intron regions were extracted from the annotation file using intronicParts function of GenomicRanges v1.50.4.

Real Time PCR

The RNA was reverse-transcribed using iScript cDNA Synthesis Kit (BioRad) and cDNA quantified with SsoAdvanced Universal SYBR Green Supermix (BioRad) following the manufacturer's protocols on a CFX96 thermal cycler (BioRad). The primer used are: HNRNPU-AS1 (AGGAAGCTGTACACTGGAGG, CAATGTCTTCACCAATAACAAAGC); HNRNPU (AGTTTAACAGAGGTGGTGGCC, GCCCCTCCTATTATATCCGCC); GAPDH (AAGGTGAAGGTCGGAGTCAAC, GGGGTCATTGATGGCAACAATA). CFX Manager software was used to record amplification curves and to determine Ct values. RT-qPCR reactions were performed in technical triplicates. We calculated the ΔCt to the GAPDH housekeeping gene and ΔΔCt to control cell lines. We used three biological replicates of cells seeded at different passages. Statistical significance between cell lines was determined with ANOVA and post hoc Tukey HSD in R (v. 4.1.2).

Hi-C sequencing

Cells were cultured as NES for D0 collection or differentiated for 28 days and harvested by briefly rinsing the cells in accutase and then incubating them with TrypLE express (Gibco) and neural isolation enzyme (ThermoFisher Scientific). Samples were then processed using the Arima-HiC kit (PMID: 29779944) according to the Arima Genomics User Guide for Mammalian Cell Lines (catalog number A510008). Briefly, we crosslinked harvested cells with 2% formaldehyde and then used approximately 1 million fixed cells as input for each replicate sample. Subsequently, we used 1.5 µg of Hi-C template for biotin pull-down and library preparation according to the Arima Genomics User Guide for Library Preparation using KAPA Hyper Prep Kit. Specifically, we used eight PCR cycles for library amplification. We then sequenced the Arima-HiC libraries for each time point on one flowcell on the Illumina NovaSeq S Prime system, obtaining an average of 900 M sequencing reads for D0 samples, and 1000 M sequencing reads per sample for D28 samples. Sequencing was carried out at the National Genomics Infrastructure at the Science for Life Laboratory (SciLifeLab) in Stockholm, Sweden.

We processed the raw sequencing reads using the HiCUP pipeline (v0.7.4) (PMID: 26835000) with default parameters. Briefly, the pipeline employs Bowtie2 (v2.4.1) (PMID: 22388286) to align the reads to the human reference genome (GRCh37/hg19) and filter out experimental artifacts (i.e. circularised, re-ligated, and duplicate reads). We generated the 'digest file' using the 'hicup_digester' command with the Arima option (–Arima). We used the HiCUP output files (BAM format), which contain only valid, non-redundant read pairs, as input for pairtools (v0.3.0). First, we converted the BAM files into .pairsam format using the pairtools parse and sort modules. In addition to individual replicates, we generated pooled samples for each developmental stage by merging replicates using the pairtools merge module. We marked read duplicates using the pairtools dedup module, with option –mark-dups, and filtered the results by selecting only specific pair types (i.e. 'U.U.', 'U.R.' and 'R.U.') via the pairtools select module, which produced a .pairs format output. Finally, we added the fragment information using the 'fragment_4dnpairs.pl' convenience script provided alongside the Juicer pipeline and converted the .pairs files into .hic format using the Pre module from Juicer-Tools (v1.22.01). Unless explicitly required by the software/package, the contact matrices were normalized to the smallest library and corrected with ICE using HiCexplorer (v3.7) (Ramírez et al., 2017). HiCexplorer package was used for mapping genomic contacts and contact enrichment between the samples.

The compartments were called at 1 Mb resolution, and the first four PCAs were extracted by HiCexplorer using the hicPCA tool and the gene track from hg19 to assure the correct orientation of the eigenvector. The PCA for each chromosome and each sample were chosen by considering the highest correlating PCA between the samples and the best mapping with the gene density eigenvector. The compartments were defined as A and B according to the eigenvector orientation, with A being the gene-rich and positive eigenvector and B being the gene-poor regions and negative eigenvector. FanC toolkit (v0.9.1) (Kruse et al., 2020) was used to calculate compartment strength and cis-trans- compartment interactions. The R package annotatr was used to annotate the genomic regions switching compartments in the different conditions.

Deconvolution

The deconvolution of bulk RNA-seq data to previously published scRNA-seq sample (Becker et al., 2020) was done using the Bseq-SC package (Baron et al., 2016). Bseq-SC uses cell-type-specific marker genes from single-cell RNA transcriptomes to predict cell-type proportions underlying bulk RNA transcriptomes. Deconvolution was done with 30 marker genes for each cell population, except for cluster 'Undefined maturing neurons', which had only 25 defining genes. Statistical differences in the estimated cell proportions were calculated by the χ^2 statistical test in R (v4.1.2).

Public data processing

Data from Human Brain Transcriptome (https://hbatlas.org) were obtained to visualize *HNRNPU* expression in different human brain regions during development. Additional stem cell time-course data was accessed via LIBD Stem Cell Browser (http://stemcell.libd.org/scb). RPKM values for HNRNPU were extracted for evaluating *HNRNPU* expression during neuronal differentiation from iPSCs (Burke et al., 2020). Seurat object for human cortical organoid data was downloaded from GEO with accession number GSE219317 (Ressler et al., 2023).

Cell proliferation assay

To analyze differences in cellular proliferation, the BrdU assay (ab126556, Abcam) was performed for three replicates at D0, D5, and D28 time points. Twenty-four hours prior to the read-out, 1X-BrdU reagent was added to the cell culture vessels for incorporation by incubation at 37°C and 5% CO_2. The culture media was aspirated for the read-out, and cells were fixed with the supplied fixing solution. This was followed by exposure to the anti-BrdU antibody (primary antibody), incubation at room temperature for 1 h, and washing with the supplied plate wash buffer. The cells were incubated with the HRP-tagged secondary antibody at room temperature for 30 min, followed by TMB exposure and recording absorbance at 450 nm. Afterwards, the cells were incubated in TBS, 0.1% Triton-X 100, and Hoechst 1:1000 for 15 min, followed by fluorescence measurement, which was used to calibrate the BrdU quantification for the number of nuclei in each sample. The quantification of proliferation rate followed by Student's *t*-test statistical comparison was done in R (v4.1.2).

Electrophysiology

Whole-cell patch-clamp recordings were performed at 5, 8, 28, and 50 days of differentiation. Immediately prior to recordings, the cells were washed with 1× PBS, and then Krebs-Ringer's solution composed of (in mM): NaCl 119, KCl 2.5, NaH2PO4 1, CaCl2 2H2O 2.5, MgCl2 6H2O 1.3, HEPES 20, D-Glucose 11 (pH 7.4)+Laminin 1:1000 was added in the dish. The recordings were performed in Krebs-Ringer's solution. Recording pipettes were fabricated with a Narishige pc-100 puller and had resistances of 3-5 MOhm when filled with the internal solution composed of (in mM): 120 K-gluconate, 0.1 EGTA, 4 MgATP, 0.3 Na2GTP, 10 HEPES, 20 KCl and 5 Na2-phosphocreatine (pH 7.4). Current and voltage responses were measured at room temperature using a MultiClamp 700B amplifier (Molecular Devices) and digitized with Axon™ Digidata® 1550B

analog-to-digital converter connected to a personal computer running pClamp 11.0.3 (Molecular Devices). Membrane capacitance and resistance were derived from the pClamp 11.0.3 (Molecular Devices) membrane-test function. Data analysis was performed by Clampfit 10.7 (Molecular Devices).

Acknowledgements
The authors are grateful to the donors of the cell lines for their participation in this research. The authors acknowledge support from the National Genomics Infrastructure in Stockholm funded by Science for Life Laboratory, the Knut and Alice Wallenberg Foundation and the Swedish Research Council. The computations and data handling were enabled by resources provided by the National Academic Infrastructure for Supercomputing in Sweden (NAISS) and the Swedish National Infrastructure for Computing (SNIC) at Uppsala Multidisciplinary Center for Advanced Computational Science, partially funded by the Swedish Research Council through grant agreements number 2022-06725 and number 2018-05973. We thank A. Smialowska at NBIS (National Bioinformatics Infrastructure Sweden) for technical support with HiC data analysis, which was made possible through application support provided by SNIC. The authors acknowledge support from the iPS Core facility at Karolinska Institutet for assistance with the generation of iPSC and NES cells.

Competing interests
M.B. is a full-time employee of Bayer AG, Germany. S.B. declares no direct conflict of interest related to this article. He discloses that he has, in the last 3 years, acted as an author, consultant, or lecturer for Medice and Roche. He receives royalties for textbooks and diagnostic tools from Hogrefe, and Liber. S.B. is shareholder in SB Education/Psychological Consulting AB and NeuroSupportSolutions International AB. The other authors have no conflicts to declare.

Author contributions
Conceptualization: F.M., M.O., and K.T.; Methodology and Data Analysis: F.M., M.O., C.S., S.A., A.A., R.B., M.M., F.A., A.P., M.W., I.R., M.B., D.L., B-M.A., J.I., K.L.R., Mo.M., Y.J., A.F., A.B., and K.T.; Validation: F.M., M.O., C.S., S.A., A.A., and K.T.; Resources: S.B. and K.T.; Data Curation: F.M., M.O., A.A., F.A., A.P., M.W., D.L., B.M.A., J.I., K.L.R.; Writing – Original Draft: F.M. and K.T.; Writing – Review & Editing: F.M., M.O., and K.T.; Visualization: F.M., M.O., D.L., and K.T.; Supervision: Y.J., N.C., M.Bi., E.S., A.B., and K.T.; Project Administration: F.M. and K.T.; Funding Acquisition: F.M., Y.J., N.C., E.S., A.B., S.B., and K.T., Critical review of the draft: All authors.

Funding
The project was supported by grants from the Swedish Research Council to K.T. (grant number 2017-01660), S.B. (grant number 2019-01303), and N.C. (grant number 2018-02950); Swedish Foundation for Strategic Research to K.T. (grant number FFL18-0104); the Swedish Brain Foundation – Hjärnfonden to K.T.; the Karolinska Institutet KID Program to N.C., KI-NIH PhD program for PhD students (M.O.), Osk. Huttunen Foundation (M.O.), Åke Wiberg Foundation to K.T.; the H.K.H. Kronprinsessan Lovisas förening för barnasjukvård och Stiftelsen Axel Tielmans minnesfond to F.M.; the Swedish Foundation for Medical Research (SSMF) to F.A.; The Foundations of Petrus och Augusta Hedlund to K.T.; the Strategic Research Area Neuroscience (StratNeuro) at Karolinska Institutet to K.T.; the Swedish Foundation for International Cooperation in Research and Higher Education (STINT) to K.T.; and the Committee for Research at Karolinska Institutet to K.T., grant number R35GM128661 from the National Institutes of Health to Y.J. (grant number R35GM128661). Open Access funding provided by Karolinska Institute: Karolinska Institutet. Deposited in PMC for immediate release.

Data availability
Further information and requests for resources and reagents should be directed to and fulfilled by the Lead Contact, Kristiina Tammimies (kristiina.tammimies@ki.se). All the related code and data matrixes are available in the GitHub https://github.com/Tammimies-Lab/HNRNPUdeficiency-Mastropasqua-et-al RNA-seq and Hi-C data will be uploaded to GEO and ENA.

First person
This article has an associated First Person interview with the two first authors of the paper.

References
Aldinger, K. A., Thomson, Z., Phelps, I. G., Haldipur, P., Deng, M., Timms, A. E., Hirano, M., Santpere, G., Roco, C., Rosenberg, A. B., et al. (2021). Spatial and cell type transcriptional landscape of human cerebellar development. *Nat. Neurosci.* **24**, 1163-1175. doi:10.1038/s41593-021-00872-y

Anders, S., Reyes, A. and Huber, W. (2012). Detecting differential usage of exons from RNA-seq data. *Genome Res.* **22**, 2008-2017. doi:10.1101/gr.133744.111

Balasubramanian, M., (2022). HNRNPU-Related neurodevelopmental disorder. In *GeneReviews®* [Internet] (ed. M. P. Adam, D. B. Everman, G. M. Mirzaa, R. A. Pagon, S. E. Wallace, L. J. Bean, K. W. Gripp and A. Amemiya). Seattle, WA: University of Washington, Seattle; 1993-2023. Available from: https://www.ncbi.nlm.nih.gov/books/NBK578573/.

Ban, R., Kopajtich, R., Lv, J., Stenton, S. L., Shimura, M., Wang, Z., Yuan, Y., Wang, J., Han, X., Liu, Z., et al. (2022). The phenotypic spectrum of COX20-associated mitochondrial disorder. *Brain* **145**, e125-e127. doi:10.1093/brain/awac344

Baron, M., Veres, A., Wolock, S. L., Faust, A. L., Gaujoux, R., Vetere, A., Ryu, J. H., Wagner, B. K., Shen-Orr, S. S., Klein, A. M., et al. (2016). A single-cell transcriptomic map of the human and mouse pancreas reveals inter- and intra-cell population structure. *Cell Syst.* **3**, 346-360.e4. doi:10.1016/j.cels.2016.08.011

Becker, M., Mastropasqua, F., Reising, J. P., Maier, S., Ho, M.-L., Rabkina, I., Li, D., Neufeld, J., Ballenberger, L., Myers, L., et al. (2020). Presynaptic dysfunction in CASK -related neurodevelopmental disorders. *Transl. Psychiatry* **10**, 1-17. doi:10.1038/s41398-020-00994-0

Bölte, S., Willfors, C., Berggren, S., Norberg, J., Poltrago, L., Mevel, K., Coco, C., Fransson, P., Borg, J., Sitnikov, R., et al. (2014). The roots of autism and ADHD twin study in Sweden (RATSS). *Twin Res. Hum. Genet.* **17**, 164-176. doi:10.1017/thg.2014.12

Bonev, B., Mendelson Cohen, N., Szabo, Q., Fritsch, L., Papadopoulos, G. L., Lubling, Y., Xu, X., Lv, X., Hugnot, J.-P., Tanay, A., et al. (2017). Multiscale 3D genome rewiring during mouse neural development. *Cell* **171**, 557-572.e24. doi:10.1016/j.cell.2017.09.043

Bramswig, N. C., Lüdecke, H.-J., Hamdan, F. F., Altmüller, J., Beleggia, F., Elcioglu, N. H., Freyer, C., Gerkes, E. H., Demirkol, Y. K., Knupp, K. G., et al. (2017). Heterozygous HNRNPU variants cause early onset epilepsy and severe intellectual disability. *Hum. Genet.* **136**, 821-834. doi:10.1007/s00439-017-1795-6

Brunet, T., Jech, R., Brugger, M., Kovacs, R., Alhaddad, B., Leszinski, G., Riedhammer, K. M., Westphal, D. S., Mahle, I., Mayerhanser, K., et al. (2021). De novo variants in neurodevelopmental disorders—experiences from a tertiary care center. *Clin. Genet.* **100**, 14-28. doi:10.1111/cge.13946

Burke, E. E., Chenoweth, J. G., Shin, J. H., Collado-Torres, L., Kim, S.-K., Micali, N., Wang, Y., Colantuoni, C., Straub, R. E., Hoeppner, D. J., et al. (2020). Dissecting transcriptomic signatures of neuronal differentiation and maturation using iPSCs. *Nat. Commun.* **11**, 462. doi:10.1038/s41467-019-14266-z

Burstein, O. and Geva, R. (2021). The brainstem-informed autism framework: early life neurobehavioral markers. *Front. Integr. Neurosci.* **15**, 759614.

Calzari, L., Barcella, M., Alari, V., Braga, D., Muñoz-Viana, R., Barlassina, C., Finelli, P., Gervasini, C., Barco, A., Russo, S., et al. (2020). Transcriptome analysis of iPSC-derived neurons from rubinstein-taybi patients reveals deficits in neuronal differentiation. *Mol. Neurobiol.* **57**, 3685-3701. doi:10.1007/s12035-020-01983-6

Chambers, S. M., Fasano, C. A., Papapetrou, E. P., Tomishima, M., Sadelain, M. and Studer, L. (2009). Highly efficient neural conversion of human ES and iPS cells by dual inhibition of SMAD signaling. *Nat. Biotechnol.* **27**, 275-280. doi:10.1038/nbt.1529

Connacher, R., Williams, M., Prem, S., Yeung, P. L., Matteson, P., Mehta, M., Markov, A., Peng, C., Zhou, X., McDermott, C. R., et al. (2022). Autism NPCs from both idiopathic and CNV 16p11.2 deletion patients exhibit dysregulation of proliferation and mitogenic responses. *Stem Cell Rep.* **17**, 1380-1394. doi:10.1016/j.stemcr.2022.04.019

Connolly, C., Takahashi, S., Miura, H., Hiratani, I., Gilbert, N., Donaldson, A. D. and Hiraga, S.-I. (2022). SAF-A promotes origin licensing and replication fork progression to ensure robust DNA replication. *J. Cell Sci.* **135**, jcs258991. doi:10.1242/jcs.258991

Consalez, G. G., Goldowitz, D., Casoni, F. and Hawkes, R. (2021). Origins, development, and compartmentation of the granule cells of the cerebellum. *Front. Neural Circuits* **14**, 611841.

Depienne, C., Nava, C., Keren, B., Heide, S., Rastetter, A., Passemard, S., Chantot-Bastaraud, S., Moutard, M.-L., Agrawal, P. B., VanNoy, G., et al. (2017). Genetic and phenotypic dissection of 1q43q44 microdeletion syndrome and neurodevelopmental phenotypes associated with mutations in ZBTB18 and HNRNPU. *Hum. Genet.* **136**, 463-479. doi:10.1007/s00439-017-1772-0

Dugger, S. A., Dhindsa, R. S., De Almeida Sampaio, G., Ressler, A. K., Rafikian, E. E., Petri, S., Letts, V. A., Teoh, J., Ye, J., Colombo, S., et al. (2020). Neurodevelopmental deficits and cell-type-specific transcriptomic perturbations in a mouse model of *HNRNPU* haploinsufficiency (preprint). *Neuroscience*.

Durkin, A., Albaba, S., Fry, A. E., Morton, J. E., Douglas, A., Beleza, A., Williams, D., Volker-Touw, C. M. L., Lynch, S. A., Canham, N., et al. (2020). Clinical findings of 21 previously unreported probands with HNRNPU-related syndrome and comprehensive literature review. *Am. J. Med. Genet. A* **182**, 1637-1654. doi:10.1002/ajmg.a.61599

Falk, A., Koch, P., Kesavan, J., Takashima, Y., Ladewig, J., Alexander, M., Wiskow, O., Tailor, J., Trotter, M., Pollard, S., et al. (2012). Capture of neuroepithelial-like stem cells from pluripotent stem cells provides a versatile

system for in vitro production of human neurons. *PLoS One* **7**, e29597. doi:10.1371/journal.pone.0029597

Fan, H., Lv, P., Huo, X., Wu, J., Wang, Q., Cheng, L., Liu, Y., Tang, Q.-Q., Zhang, L., Zhang, F., et al. (2018). The nuclear matrix protein HNRNPU maintains 3D genome architecture globally in mouse hepatocytes. *Genome Res.* **28**, 192-202. doi:10.1101/gr.224576.117

Focșa, I. O., Budișteanu, M. and Bălgrădean, M. (2021). Clinical and genetic heterogeneity of primary ciliopathies (Review). *Int. J. Mol. Med.* **48**, 176. doi:10.3892/ijmm.2021.5009

Frosch, I. R., Mittal, V. A. and D'Mello, A. M. (2022). Cerebellar contributions to social cognition in ASD: a predictive processing framework. *Front. Integr. Neurosci.* **16**, 810425. doi:10.3389/fnint.2022.810425

Gandal, M. J., Zhang, P., Hadjimichael, E., Walker, R. L., Chen, C., Liu, S., Won, H., van Bakel, H., Varghese, M., Wang, Y., et al. (2018). Transcriptome-wide isoform-level dysregulation in ASD, schizophrenia, and bipolar disorder. *Science* **362**, eaat8127. doi:10.1126/science.aat8127

Gillentine, M. A., Wang, T., Hoekzema, K., Rosenfeld, J., Liu, P., Guo, H., Kim, C. N., De Vries, B. B. A., Vissers, L. E. L. M., Nordenskjold, M., et al. (2021). Rare deleterious mutations of HNRNP genes result in shared neurodevelopmental disorders. *Genome Med.* **13**, 63. doi:10.1186/s13073-021-00870-6

Guo, J., Otis, J. M., Suciu, S. K., Catalano, C., Xing, L., Constable, S., Wachten, D., Gupton, S., Lee, J., Lee, A., et al. (2019). Primary cilia signaling promotes axonal tract development and is disrupted in joubert syndrome-related disorders models. *Dev. Cell* **51**, 759-774.e5. doi:10.1016/j.devcel.2019.11.005

Hu, B., Won, H., Mah, W., Park, R. B., Kassim, B., Spiess, K., Kozlenkov, A., Crowley, C. A., Pochareddy, S., PsychENCODE Consortium et al. (2021). Neuronal and glial 3D chromatin architecture informs the cellular etiology of brain disorders. *Nat. Commun.* **12**, 3968. doi:10.1038/s41467-021-24243-0

Huelga, S. C., Vu, A. Q., Arnold, J. D., Liang, T. Y., Liu, P. P., Yan, B. Y., Donohue, J. P., Shiue, L., Hoon, S., Brenner, S., et al. (2012). Integrative genome-wide analysis reveals cooperative regulation of alternative splicing by hnRNP proteins. *Cell Rep.* **1**, 167-178. doi:10.1016/j.celrep.2012.02.001

Jones, A. N., Graß, C., Meininger, I., Geerlof, A., Klostermann, M., Zarnack, K., Krappmann, D. and Sattler, M. (2022). Modulation of pre-mRNA structure by hnRNP proteins regulates alternative splicing of MALT1. *Sci. Adv.* **8**, eabp9153. doi:10.1126/sciadv.abp9153

Joseph, R. (2000). Fetal brain behavior and cognitive development. . *Dev. Rev.* **20**, 81-98. doi:10.1006/drev.1999.0486

Kiledjian, M. and Dreyfuss, G. (1992). Primary structure and binding activity of the hnRNP U protein: binding RNA through RGG box. *EMBO J.* **11**, 2655-2664. doi:10.1002/j.1460-2075.1992.tb05331.x

Kim, D. and Ackerman, S. L. (2011). The UNC5C netrin receptor regulates dorsal guidance of mouse hindbrain axons. *J. Neurosci.* **31**, 2167-2179. doi:10.1523/JNEUROSCI.5254-10.2011

Kim, D., Im, J. O., Won, Y. J., Yoon, S. Y., Lee, E. J., Lee, J. H. and Hong, H. N. (2003). Upregulation of c-Kit receptor and stem cell factor in cerebellar inhibitory synapses in response to kainic acid. *J. Neurosci. Res.* **71**, 72-78. doi:10.1002/jnr.10466

Kohlmeier, K. A. and Polli, F. S. (2020). Plasticity in the brainstem: prenatal and postnatal experience can alter Laterodorsal Tegmental (LDT) structure and function. *Front. Synaptic. Neurosci.* **12**, 3. doi:10.3389/fnsyn.2020.00003

Kruse, K., Hug, C. B. and Vaquerizas, J. M. (2020). FAN-C: a feature-rich framework for the analysis and visualisation of chromosome conformation capture data. *Genome Biol.* **21**, 303. doi:10.1186/s13059-020-02215-9

Lalli, M. A., Avey, D., Dougherty, J. D., Milbrandt, J. and Mitra, R. D. (2020). High-throughput single-cell functional elucidation of neurodevelopmental disease-associated genes reveals convergent mechanisms altering neuronal differentiation. *Genome Res.* **30**, 1317-1331. doi:10.1101/gr.262295.120

Leduc, M. S., Chao, H.-T., Qu, C., Walkiewicz, M., Xiao, R., Magoulas, P., Pan, S., Beuten, J., He, W., Bernstein, J. A., et al. (2017). Clinical and molecular characterization of de novo loss of function variants in HNRNPU. *Am. J. Med. Genet. A* **173**, 2680-2689. doi:10.1002/ajmg.a.38388

Liao, Y., Wang, J., Jaehnig, E. J., Shi, Z. and Zhang, B. (2019). WebGestalt 2019: gene set analysis toolkit with revamped UIs and APIs. *Nucleic Acids Res.* **47**, W199-W205. doi:10.1093/nar/gkz401

Lieberman-Aiden, E., van Berkum, N. L., Williams, L., Imakaev, M., Ragoczy, T., Telling, A., Amit, I., Lajoie, B. R., Sabo, P. J., Dorschner, M. O., et al. (2009). Comprehensive mapping of long-range interactions reveals folding principles of the human genome. *Science* **326**, 289-293. doi:10.1126/science.1181369

London, E., Jure, R., Gaspar, P., Puelles, L. and Kulesza, R. J. (2022). Editorial: The role of the brainstem and cerebellum in autism and related neurodevelopmental disorders (DD). *Front. Integr. Neurosci.* **16**, 957003. doi:10.3389/fnint.2022.957003

Love, M. I., Huber, W. and Anders, S. (2014). Moderated estimation of fold change and dispersion for RNA-seq data with DESeq2. *Genome Biol.* **15**, 550. doi:10.1186/s13059-014-0550-8

Lowenstein, E. D., Cui, K. and Hernandez-Miranda, L. R. (2022). Regulation of early cerebellar development. *FEBS J.* **290**, 2786-2804. doi:10.1111/febs.16426

Ma, N., Matsunaga, S., Morimoto, A., Sakashita, G., Urano, T., Uchiyama, S. and Fukui, K. (2011). The nuclear scaffold protein SAF-A is required for kinetochore–microtubule attachment and contributes to the targeting of Aurora-A to mitotic spindles. *J. Cell Sci.* **124**, 394-404. doi:10.1242/jcs.063347

Mancarci, B. O., Toker, L., Tripathy, S. J., Li, B., Rocco, B., Sibille, E. and Pavlidis, P. (2017). Cross-laboratory analysis of brain cell type transcriptomes with applications to interpretation of bulk tissue data. *eNeuro* **4**, ENEURO.0212-17.2017. doi:10.1523/ENEURO.0212-17.2017

Marchetto, M. C., Belinson, H., Tian, Y., Freitas, B. C., Fu, C., Vadodaria, K. C., Beltrao-Braga, P. C., Trujillo, C. A., Mendes, A. P. D., Padmanabhan, K., et al. (2017). Altered proliferation and networks in neural cells derived from idiopathic autistic individuals. *Mol. Psychiatry* **22**, 820-835. doi:10.1038/mp.2016.95

Marenda, M., Lazarova, E. and Gilbert, N. (2022). The role of SAF-A/hnRNP U in regulating chromatin structure. *Curr. Opin. Genet. Dev.* **72**, 38-44. doi:10.1016/j.gde.2021.10.008

Markenscoff-Papadimitriou, E., Binyameen, F., Whalen, S., Price, J., Lim, K., Ypsilanti, A. R., Catta-Preta, R., Pai, E. L.-L., Mu, X., Xu, D., et al. (2021). Autism risk gene POGZ promotes chromatin accessibility and expression of clustered synaptic genes. *Cell Rep.* **37**, 110089. doi:10.1016/j.celrep.2021.110089

McLeay, R. C. and Bailey, T. L. (2010). Motif Enrichment Analysis: a unified framework and an evaluation on ChIP data. *BMC Bioinformatics* **11**, 165. doi:10.1186/1471-2105-11-165

Merico, D., Isserlin, R., Stueker, O., Emili, A. and Bader, G. D. (2010). Enrichment map: a network-based method for gene-set enrichment visualization and interpretation. *PLoS One* **5**, e13984. doi:10.1371/journal.pone.0013984

Mowat, D., Wilson, M. and Goossens, M. (2003). Mowat-Wilson syndrome. *J. Med. Genet.* **40**, 305-310. doi:10.1136/jmg.40.5.305

Niu, Z., Wang, F., Lv, S., Lv, Y., Liu, M., Fu, L., Yao, Y., Wang, L., Lin, W. and Yuan, F. (2021). HNRNPU-AS1 regulates cell proliferation and apoptosis via the MicroRNA 205-5p/AXIN2 Axis and Wnt/b-catenin signaling pathway in cervical cancer. *Mol. Cell. Biol.* **41**, e0011521. doi:10.1128/MCB.00115-21

Nozawa, R.-S., Boteva, L., Soares, D. C., Naughton, C., Dun, A. R., Buckle, A., Ramsahoye, B., Bruton, P. C., Saleeb, R. S., Arnedo, M., et al. (2017). SAF-A regulates interphase chromosome structure through oligomerization with chromatin-associated RNAs. *Cell* **169**, 1214-1227.e18. doi:10.1016/j.cell.2017.05.029

Parisian, A. D., Koga, T., Miki, S., Johann, P. D., Kool, M., Crawford, J. R. and Furnari, F. B. (2020). SMARCB1 loss interacts with neuronal differentiation state to block maturation and impact cell stability. *Genes Dev.* **34**, 1316-1329. doi:10.1101/gad.339978.120

Paulsen, B., Velasco, S., Kedaigle, A. J., Pigoni, M., Quadrato, G., Deo, A., Adiconis, X., Uzquiano, A., Kim, K., Simmons, S. K., et al. (2020). Human brain organoids reveal accelerated development of cortical neuron classes as a shared feature of autism risk genes. *bioRxiv*, 2020.11.10.376509. doi:10.1101/2020.11.10.376509

Pilaz, L.-J., McMahon, J. J., Miller, E. E., Lennox, A. L., Suzuki, A., Salmon, E. and Silver, D. L. (2016). Prolonged mitosis of neural progenitors alters cell fate in the developing brain. *Neuron* **89**, 83-99. doi:10.1016/j.neuron.2015.12.007

Poulet, A., Arganda-Carreras, I., Legland, D., Probst, A. V., Andrey, P. and Tatout, C. (2015). NucleusJ: an ImageJ plugin for quantifying 3D images of interphase nuclei. *Bioinformatics* **31**, 1144-1146. doi:10.1093/bioinformatics/btu774

Ramírez, F., Bhardwaj, V., Villaveces, J., Arrigoni, L., Grüning, B. A., Lam, K. C., Habermann, B., Akhtar, A. and Manke, T. (2017). High-resolution TADs reveal DNA sequences underlying genome organization in flies. *Nat. Commun.* **9**, 189. doi:10.1101/115063

Reimand, J., Isserlin, R., Voisin, V., Kucera, M., Tannus-Lopes, C., Rostamianfar, A., Wadi, L., Meyer, M., Wong, J., Xu, C., et al. (2019). Pathway enrichment analysis and visualization of omics data using g:Profiler, GSEA, Cytoscape and EnrichmentMap. *Nat. Protoc.* **14**, 482-517. doi:10.1038/s41596-018-0103-9

Ressler, A. K., Sampaio, G. L. A., Dugger, S. A., Sapir, T., Krizay, D., Boland, M. J., Reiner, O. and Goldstein, D. B. (2023). Evidence of shared transcriptomic dysregulation of HNRNPU-related disorder between human organoids and embryonic mice. *iScience* **26**, 105797. doi:10.1016/j.isci.2022.105797

Roshon, M. J. and Ruley, H. E. (2005). Hypomorphic mutation in hnRNP U results in post-implantation lethality. *Transgenic Res.* **14**, 179-192. doi:10.1007/s11248-004-8147-8

Sapir, T., Kshirsagar, A., Gorelik, A., Olender, T., Porat, Z., Scheffer, I. E., Goldstein, D. B., Devinsky, O. and Reiner, O. (2022). Heterogeneous nuclear ribonucleoprotein U (HNRNPU) safeguards the developing mouse cortex. *Nat. Commun.* **13**, 4209. doi:10.1038/s41467-022-31752-z

Satterstrom, F. K., Kosmicki, J. A., Wang, J., Breen, M. S., De Rubeis, S., An, J.-Y., Peng, M., Collins, R., Grove, J., Klei, L., et al. (2020). Large-scale exome sequencing study implicates both developmental and functional changes in the neurobiology of autism. *Cell* **180**, 568-584.e23. doi:10.1016/j.cell.2019.12.036

Shannon, P., Markiel, A., Ozier, O., Baliga, N. S., Wang, J. T., Ramage, D., Amin, N., Schwikowski, B. and Ideker, T. (2003). Cytoscape: a software environment

for integrated models of biomolecular interaction networks. *Genome Res.* **13**, 2498-2504. doi:10.1101/gr.1239303

Sharp, J. A., Perea-Resa, C., Wang, W. and Blower, M. D. (2020). Cell division requires RNA eviction from condensing chromosomes. *J. Cell Biol.* **219**, e201910148. doi:10.1083/jcb.201910148

Shimojima, K., Okamoto, N., Suzuki, Y., Saito, M., Mori, M., Yamagata, T., Momoi, M. Y., Hattori, H., Okano, Y., Hisata, K., et al. (2012). Subtelomeric deletions of 1q43q44 and severe brain impairment associated with delayed myelination. *J. Hum. Genet.* **57**, 593-600. doi:10.1038/jhg.2012.77

Spahiu, L., Behluli, E., Grajçevci-Uka, V., Liehr, T. and Temaj, G. (2022). Joubert syndrome: Molecular basis and treatment. *J. Mother Child* **26**, 118-123. doi:10.34763/jmotherandchild.20222601.d-22-00034

Stamouli, S., Anderlid, B.-M., Willfors, C., Thiruvahindrapuram, B., Wei, J., Berggren, S., Nordgren, A., Scherer, S. W., Lichtenstein, P., Tammimies, K., et al. (2018). Copy number variation analysis of 100 twin pairs enriched for neurodevelopmental disorders. *Twin Res. Hum. Genet.* **21**, 1-11. doi:10.1017/thg.2017.69

Su, C., Argenziano, M., Lu, S., Pippin, J. A., Pahl, M. C., Leonard, M. E., Cousminer, D. L., Johnson, M. E., Lasconi, C., Wells, A. D., et al. (2021). 3D promoter architecture re-organization during iPSC-derived neuronal cell differentiation implicates target genes for neurodevelopmental disorders. *Prog. Neurobiol.* **201**, 102000. doi:10.1016/j.pneurobio.2021.102000

Taylor, J., Spiller, M., Ranguin, K., Vitobello, A., Philippe, C., Bruel, A.-L., Cappuccio, G., Brunetti-Pierri, N., Willems, M., Isidor, B., et al. (2022). Expanding the phenotype of HNRNPU-related neurodevelopmental disorder with emphasis on seizure phenotype and review of literature. *Am. J. Med. Genet.* **188**, 1497-1514. doi:10.1002/ajmg.a.62677

Thierry, G., Bénéteau, C., Pichon, O., Flori, E., Isidor, B., Popelard, F., Delrue, M.-A., Duboscq-Bidot, L., Thuresson, A.-C., van Bon, B. W. M., et al. (2012). Molecular characterization of 1q44 microdeletion in 11 patients reveals three candidate genes for intellectual disability and seizures. *Am. J. Med. Genet. A* **158A**, 1633-1640. doi:10.1002/ajmg.a.35423

Tung, Y., Lu, H., Lin, W., Huang, T., Kim, S., Hu, G., Zhang, G. and Zheng, G. (2021). Case report: identification of a de novo microdeletion 1q44 in a patient with seizures and developmental delay. *Front. Genet.* **12**, 648351. doi:10.3389/fgene.2021.648351

Uhlin, E., Marin Navarro, A., Rönnholm, H., Day, K., Kele, M. and Falk, A. (2017a). Integration free derivation of human induced pluripotent stem cells using laminin 521 matrix. *J. Vis. Exp.*, 56146.

Uhlin, E., Rönnholm, H., Day, K., Kele, M., Tammimies, K., Bölte, S. and Falk, A. (2017b). Derivation of human iPS cell lines from monozygotic twins in defined and xeno free conditions. *Stem Cell Res.* **18**, 22-25. doi:10.1016/j.scr.2016.12.006

Wang, T., Hoekzema, K., Vecchio, D., Wu, H., Sulovari, A., Coe, B. P., Gillentine, M. A., Wilfert, A. B., Perez-Jurado, L. A., Kvarnung, M., et al. (2020). Large-scale targeted sequencing identifies risk genes for neurodevelopmental disorders. *Nat. Commun.* **11**, 4932. doi:10.1038/s41467-020-18723-y

Wu, B., Blot, F. G., Wong, A. B., Osório, C., Adolfs, Y., Pasterkamp, R. J., Hartmann, J., Becker, E. B., Boele, H.-J., De Zeeuw, C. I., et al. (2019). TRPC3 is a major contributor to functional heterogeneity of cerebellar Purkinje cells. *Elife* **8**, e45590. doi:10.7554/eLife.45590

Xiao, R., Tang, P., Yang, B., Huang, J., Zhou, Y., Shao, C., Li, H., Sun, H., Zhang, Y. and Fu, X.-D. (2012). Nuclear matrix factor hnRNP U/SAF-A exerts a global control of alternative splicing by regulating U2 snRNP maturation. *Mol. Cell* **45**, 656-668. doi:10.1016/j.molcel.2012.01.009

Xiong, J., Liu, T., Mi, L., Kuang, H., Xiong, X., Chen, Z., Li, S. and Lin, J. D. (2020). hnRNPU/TrkB Defines a chromatin accessibility checkpoint for liver injury and nonalcoholic steatohepatitis pathogenesis. *Hepatology* **71**, 1228-1246. doi:10.1002/hep.30921

Yates, T. M., Vasudevan, P., Chandler, K. E., Donnelly, D. E., Stark, Z., Sadedin, S., Willoughby, J. and Balasubramanian, M. (2017). De Novo mutations in HNRNPU result in a neurodevelopmental syndrome. *Am. J. Med. Genet. A* **173**, 3003-3012. doi:10.1002/ajmg.a.38492

Ye, J., Beetz, N., O'Keeffe, S., Tapia, J. C., Macpherson, L., Chen, W. V., Bassel-Duby, R., Olson, E. N. and Maniatis, T. (2015). hnRNP U protein is required for normal pre-mRNA splicing and postnatal heart development and function. *Proc. Natl. Acad. Sci. U.S.A.* **112**, E3020-E3029. doi:10.1073/pnas.1508461112

Zhang, X., Chen, M. H., Wu, X., Kodani, A., Fan, J., Doan, R., Ozawa, M., Ma, J., Yoshida, N., Reiter, J. F., et al. (2016). Cell-type-specific alternative splicing governs cell fate in the developing cerebral cortex. *Cell* **166**, 1147-1162.e15. doi:10.1016/j.cell.2016.07.025

Zhang, L., Zhao, Y., Guan, H. and Zhang, D. (2022). HnRNPU-AS1 inhibits the proliferation, migration and invasion of HCC cells and induces autophagy through miR-556-3p/ miR-580-3p/SOCS6 axis. *Cancer Biomark.* **34**, 443-457. doi:10.3233/CBM-210261

Zietzer, A., Hosen, M. R., Wang, H., Goody, P. R., Sylvester, M., Latz, E., Nickenig, G., Werner, N. and Jansen, F. (2020). The RNA-binding protein hnRNPU regulates the sorting of microRNA-30c-5p into large extracellular vesicles. *J. Extracell. Vesicles* **9**, 1786967. doi:10.1080/20013078.2020.1786967

Zucco, A. J., Dal Pozzo, V., Afinogenova, A., Hart, R. P., Devinsky, O. and Arcangelo, G. D. (2018). Neural progenitors derived from Tuberous Sclerosis Complex patients exhibit attenuated PI3K/AKT signaling and delayed neuronal differentiation. *Mol. Cell. Neurosci.* **92**, 149-163. doi:10.1016/j.mcn.2018.08.004